

# The Loading and Storage of Li and Rb in an Optical Dipole Trap

by

Will Gunton

A THESIS SUBMITTED IN PARTIAL FULFILLMENT OF  
THE REQUIREMENTS FOR THE DEGREE OF

BACHELOR OF SCIENCE

in

The Faculty of Science

(Physics)

THE UNIVERSITY OF BRITISH COLUMBIA

(Vancouver)

June 2009

© Will Gunton 2009

# Abstract

An optical dipole trap for Lithium and Rubidium was built from a 100W fibre laser operating at a wavelength of 1090nm. The trap consists of two single beam arms with a waist of  $37\mu\text{m}$  and  $46\mu\text{m}$ , which cross at their focus and at the focus of a second trapping laser. The physics behind the transfer of atoms into the trap from a MOT was studied through various loading models and parameters, with the aim to increase the transfer efficiency and maximize density. The effects of varying load time, hold time, trapping power, MOT size, and the radial trapping frequencies were examined and documented. The final design is capable of 40W of power, with the ability to transfer a minimum of 40% of the Rb atoms in a MOT to the dipole trap, with lifetimes on the order of 3-5 seconds. Trapping Li is left for future work, but is theoretically achievable in the current setup.

# Table of Contents

<b>Abstract</b> . . . . .	ii
<b>Table of Contents</b> . . . . .	iii
<b>List of Tables</b> . . . . .	v
<b>List of Figures</b> . . . . .	vi
<b>Acknowledgements</b> . . . . .	viii
<b>Thesis</b>	ix
<b>1 Introduction and Motivation</b> . . . . .	1
<b>2 Optical Dipole Trap Theory</b> . . . . .	4
2.1 Classical Model . . . . .	4
2.1.1 Polarizability . . . . .	4
2.1.2 Dipole Potential . . . . .	5
2.1.3 Scattering Rate . . . . .	5
2.1.4 Scaling in Certain Limits . . . . .	6
2.2 Semi-Classical Model . . . . .	8
2.2.1 Decay Rate . . . . .	8
2.2.2 Stark Shift . . . . .	9
2.2.3 Multi-Level Atom . . . . .	10
2.3 Gaussian Beam Trap . . . . .	11
<b>3 Laser Characterization</b> . . . . .	14
3.1 Calibration . . . . .	14
3.2 Power Spectrum . . . . .	14
3.3 Power Fluctuations . . . . .	14
3.3.1 In Phase Oscillations . . . . .	16
3.3.2 Out of Phase Oscillations . . . . .	16
3.4 Relaxation Oscillations . . . . .	17
3.5 Beam Distortion . . . . .	19
3.6 Cell Absorption and Reflection . . . . .	23
3.7 Detailed Image Analysis . . . . .	24
3.8 Other Materials . . . . .	26
3.9 Cell Damage . . . . .	26

*Table of Contents*

---

3.10 Calculations . . . . .	26
<b>4 Experimental Setup . . . . .</b>	<b>28</b>
4.1 Cross Beam Trap Design . . . . .	28
4.2 Imaging . . . . .	29
4.2.1 Rb85 Atom Number to Fluorescence Calibration . . . . .	29
<b>5 Results . . . . .</b>	<b>33</b>
5.1 Trap Alignment . . . . .	33
5.2 Trap Parameters . . . . .	35
5.2.1 Radial Trap Frequencies . . . . .	35
5.2.2 Hold Times . . . . .	37
5.2.3 Atom Number vs. MOT Size . . . . .	39
5.2.4 Atom Number vs. Load Time . . . . .	40
5.2.5 Atom Number vs. Power . . . . .	42
<b>6 Future Considerations . . . . .</b>	<b>49</b>
<b>7 Conclusions . . . . .</b>	<b>50</b>
<b>Bibliography . . . . .</b>	<b>51</b>
 <b>Appendices</b>	
<b>A Experimental Setup Schematic . . . . .</b>	<b>52</b>
<b>B Rb85 Atom Number to Fluorescence Calibration Calculations . . . . .</b>	<b>53</b>
<b>C Trap Depth and Frequency Calculation . . . . .</b>	<b>57</b>

# List of Tables

3.1	Predicted and Measured values for beam focus using 200mm lens . . . . .	27
3.2	Trap Depth and Frequency calculations for $^{85}\text{Rb}$ . . . . .	27
4.1	Power loss of MOT beam due to MOT cell . . . . .	31
4.2	Intensity of each MOT beam at the MOT center. . . . .	31
5.1	Initial loading rates . . . . .	42
5.2	Effective detuning during loading . . . . .	44

# List of Figures

1.1	Cartoon setup of a MOT	2
2.1	Optical dipole trap formed by a focused Gaussian beam	6
2.2	Energy level structure of an alkali atom	8
2.3	Effect of red detuned light on atomic energy levels	10
2.4	Schematic of a Gaussian beam profile	11
3.1	Laser output power response to input voltage	15
3.2	Power spectrum of SPI Laser at various powers	16
3.3	Photodiode noise	17
3.4	In phase power fluctuations at 210kHz	18
3.5	In phase power fluctuations at 30Hz	19
3.6	Out of phase power fluctuations (low power) at 910Hz	20
3.7	Out of phase power fluctuations (high power)	21
3.8	Relaxation Oscillations	22
3.9	Distortion threshold power as a function of beam focus location	23
3.10	Beam distortion with increasing power	24
3.11	Beam distortion with clean beam subtracted	25
3.12	Summed pixel count as a measure of distortion	25
3.13	Beam distortion as a function of time	25
3.14	Effect of 4mm Quartz slab on beam	26
3.15	Cell damage seen on absorption image	27
4.1	Rb photodiode calibration	30
4.2	Relationship between recapture pixel count and photodetector output voltage	32
5.1	Triangulated cross trap	34
5.2	Three beam cross trap	34
5.3	Crossing of IPG and SPI Beam One	35
5.4	Crossing of IPG and SPI Beam Two	36
5.5	Crossing of the two SPI beams	37
5.6	Radial trap frequencies for single arm trap	38
5.7	Radial trap frequencies for cross beam trap	38
5.8	Trap lifetimes for single arm trap	39
5.9	Trap lifetimes for cross beam trap	40
5.10	Trap number versus MOT Size for single arm trap	41
5.11	Trap number versus MOT Size for cross beam trap	41
5.12	Loading curve for single arm traps	43
5.13	Loading curve for cross trap at 15w and 30W	44

*List of Figures*

---

5.14	Atom number versus power for single arm traps . . . . .	45
5.15	Atom number versus power for cross beam trap . . . . .	46
5.16	Effect of changing hold time on atom number versus power curve . . . . .	46
5.17	Cartoon of the effect of the AC Stark Shift in the dipole trap . . . . .	47
5.18	Effect of changing pump detuning on atom number versus power curve . . . . .	47
5.19	Effect of changing repump detuning on atom number versus power curve . . . . .	48

# Acknowledgements

I owe a great deal of thanks to Ben Deh and Alan Robinson for their help and guidance in this project. To Janelle Van Dongen for her willingness and never ending patience to explain the obvious and Bruce Klappauf for being an immeasurable source of knowledge, teaching me that Friday nights really are best spent in a basement and that every problem has a solution.

Finally, none of this would be possible without the help of Kirk Madison. His love of physics and discovery single handily helped me discover my love of physics, and willingness to teach and explain is unparalleled. Thank you for the amazing opportunity, all your time and effort, and extraordinary enthusiasm for science.

# Thesis

# Chapter 1

## Introduction and Motivation

Over the last fifteen years, the study of ultracold atoms has had a large impact in the field of physics, highlighted by the formation of the Bose-Einstein Condensate in 1995. As interest in the study and control of complex quantum systems continues to increase, ultracold molecules may pave the way to new possibilities. The creation and study of phenomena related to cold molecules require dense, very low temperature samples of atomic species. Optical dipole traps are the near ideal tool to meet these requirements, as they allow for the detailed control of the trapping potential, and have the ability to trap any polarizable particle, atomic species, or even molecules. Within these traps, cold molecules can be created and studied from cold atoms through photoassociation, Feshbach resonances, and the creation of molecular Bose-Einstein Condensates.

Traditionally, a magneto-optical trap (MOT) (see [1] for a full description) is used to simultaneously compress and cool atoms to very low temperatures. MOT's provide cooling through velocity dampening due to the Doppler Effect, while at the same time providing spatial control via an inhomogeneous magnetic field (increasing from zero radially outward from the trap center). The magnetic field introduces a Zeeman Shift on the atoms energy levels, moving the optical resonance closer to one of two detuned counter propagating laser beams, and away from the other (in 1D). This provides a spatially dependant force that drives atoms towards the trap center, where the magnetic field is zero [Fig. 1.1]. Unfortunately, because the cooling depends on a closed two level energy loop, laser cooling and MOT's are not effective for molecules, which can have a much more complex structure of energy levels [2]. Instead, a process known as photoassociation can be used to create cold molecules from cold atoms.

Photoassociation is a process in which two atoms collide and absorb a photon (at the proper frequency) to create a bound molecule in an excited state. Colder samples of atoms provide a smaller spread in kinetic energies. This results in a smaller spread of optical frequencies that can drive the resonant photoassociation, leading to a reduction of the effect of Doppler broadening. Once in the excited state, the molecule can decay back into two free atoms (and an associated photon) or into a molecular bound state. Since an ultracold atomic sample will produce ultracold molecules (even if only on a transient basis), there is no requirement for optically cooling of the molecule itself. Full details on photoassociation can be found in [3]. More photoassociated molecules, and sharper resonance lines can be formed by increasing collision rates through higher densities and lower temperatures inside the optical trap. This can be (relatively) easily achieved in an optical dipole trap through many different methods, including:

**Evaporative Cooling** Natural evaporative cooling occurs when elastic collisions with atoms from outside the trap increase the energy of the trapped particles high enough to allow them to escape from the trapping potential. This process can be forced by the selective removal of high energy atoms in a dipole trap by decreasing the trapping depth such that the high

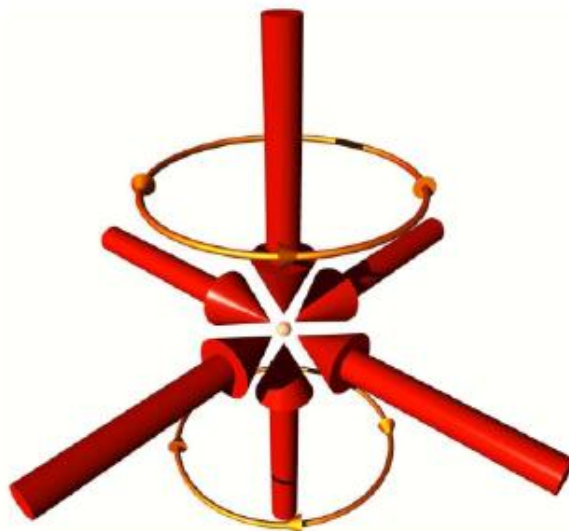


Figure 1.1: Cartoon setup of a MOT. Arrows provide cooling in 3D due to Doppler cooling, while the magnetic field coils in an Anti-Helmholtz configuration producing a spatially varying magnetic field that produces a position dependent radiation pressure that confines atoms to the center of the trap. Figure from [6].

energy particles escape. Rethermalization then occurs via elastic collisions, resulting in a lower equilibrium temperature of the sample. In order for evaporative cooling to work efficiently, high initial loading densities are required to allow for fast rethermalization rates (since the cooling rate must be large compared to heating and loss rates), and to compensate for large loss numbers [4]

**Sympathetic Cooling** Some atomic species (Lithium being a prime example) are not good candidates for evaporative cooling because of a relatively high initial temperature imposed by the MOT (leading to very large losses in evaporative cooling), low scattering lengths (leading to long rethermalization times) or no scattering at all due to the Pauli exclusion principle. In order to cool well past the limit of doppler cooling, these atoms are brought into contact with another atomic species that can be cooled easily through other methods. Collisions between the two species create a new equilibrium distribution of energies for each atom, which causes a loss in the warmer species due to evaporation. It is this rethermalization between the two species that creates a new (lower) equilibrium temperature for the warm species. Further details and an applicable example involving Li and Cs can be found in [5].

More broadly, and perhaps most intriguingly, the dipole trap can be used to create Bose-Einstein Condensates or fermionic condensates from either trapped atomic species or molecules. Aside from the realization of quantum effects on a macroscopic scale, these two new states of matter may offer an interesting link between two realms of the physics world - low temperature condensed matter and astrophysics. There is a potential to model white dwarf stars (made up of electron degenerate matter), neutron stars (acting as a superfluid), black holes (via the flow of a BEC through a constriction where the flow velocity can exceed the sound velocity) and a possi-

ble link between supernova explosions and the so called "bosenova" created by rapidly cycling a external magnetic field across a Feshbach resonance.

This thesis details and highlights the construction and characterization of an optical dipole trap for Li and Rb, in order to optimize the transfer of atoms from a MOT and maximize the density (and number of) atoms contained within the trap. The trap in question is built out of a 100 Watt fibre laser operating at a wavelength of 1090nm, split into two seperate beam arms, focused to spot sizes of  $37\mu\text{m}$  and  $46\mu\text{m}$ . Although the only trapping achieved at this point in time involves Rb, the setup and optimization is done keeping in mind the end goal of achieving trapped lithium.

# Chapter 2

## Optical Dipole Trap Theory

Optical dipole traps operate on the basis of (in the classical approach) an induced dipole potential resulting from the interaction of an atom with laser light. Alternatively, from the viewpoint of quantum mechanics, there is an optically induced downward shift in the ground state energy of an atom, known as the AC Stark Shift [4]. In reality, the interaction of light with matter actually produces two types of mechanical forces: The dipole force is responsible for the trapping potential while the radiation pressure force (due to inelastic collisions of atoms) is responsible for the heating of atoms, leading to trap loss. For comparison, this radiation pressure force is used as the cooling force in the MOT. The physics of both forces will be discussed, starting with the classical approach and followed with the semi-classical approach, which takes into account the discrete nature of energy levels within an atom.

### 2.1 Classical Model

#### 2.1.1 Polarizability

We start by considering the Lorenz Model of the atom as a damped harmonic oscillator interacting with monochromatic light given by:

$$\mathbf{E}^{(+)}(t) = -\hat{\varepsilon}E_o^{(+)}e^{-i\omega t} \quad (2.1)$$

where  $\hat{\varepsilon}$  is the unit polarization vector, and the superscript  $(+)$  serves as a reminder that there is a corresponding negative frequency term, such that  $\mathbf{E} = \mathbf{E}^{(+)} + \mathbf{E}^{(-)}$  since the  $\mathbf{E}$  field is real. This model makes use of the dipole approximation, which assumes that the size of the atom is much smaller than the wavelength of the incident light. With this approximation, the electron only sees the field at the nuclear position, and no spatial dependence of the field-atom interaction is required. Thus, since the force on the electron is  $\mathbf{F}^{(+)} = -e\mathbf{E}^{(+)}$ , the equation of motion for the moving electron is:

$$m\ddot{x} + m\gamma\omega\dot{x} + m\omega_o^2x = -\hat{\varepsilon}E_o^{(+)}e^{-i\omega t} \quad (2.2)$$

with the solution:

$$\mathbf{x}^{(+)}(t) = \hat{\varepsilon}x_o e^{-i\omega t} \quad (2.3)$$

where

$$x_o^{(+)} = \frac{eE_o^{(+)}/m}{\omega^2 - \omega_o^2 + i\gamma\omega} \quad (2.4)$$

At this point, it is important to point out that  $\omega$  is the frequency of incident light, and  $\omega_o$  is the oscillation frequency of the electron (which is referred to as the resonance frequency). Also

note that the dampening coefficient ( $\gamma_\omega$ ) has a frequency dependency. The incident light induces an electric dipole in the atom, with a dipole moment given by:

$$\mathbf{d}^{(+)} = -e\mathbf{x}^{(+)} = \alpha(\omega)\mathbf{E}^{(+)} \quad (2.5)$$

where  $\alpha(\omega)$  is the frequency dependant polarizability which gives a measure of how easily the incident light induces a dipole moment. Its value is given by:

$$\alpha(\omega) = \frac{\mathbf{d}^{(+)}}{\mathbf{E}^{(+)}} = \frac{e^2/m}{\omega^2 - \omega_o^2 - i\gamma_\omega\omega} \quad (2.6)$$

The polarizability is complex, and can be separated into a real part and an imaginary part:

$$Re[\alpha(\omega)] = \frac{e^2}{m} \frac{(\omega_o^2 - \omega^2)}{(\omega_o^2 - \omega^2)^2 + \gamma_\omega^2\omega^2} \quad (2.7)$$

$$Im[\alpha(\omega)] = \frac{e^2}{m} \frac{\gamma_\omega^2\omega}{(\omega_o^2 - \omega^2)^2 + \gamma_\omega^2\omega^2} \quad (2.8)$$

### 2.1.2 Dipole Potential

The interaction of the dipole moment (2.6) with the incident light induces a dipole potential given by:

$$V_{\text{dip}} = \frac{-\mathbf{d} \cdot \mathbf{E}}{2} \quad (2.9)$$

where the factor  $\frac{1}{2}$  comes from the fact the dipole is induced [6]. Both the positive and negative frequency contributions to the dipole moment and the electric field terms must be included. However, the  $\mathbf{d}^{(\pm)} \cdot \mathbf{E}^{(\pm)}$  terms rotate quickly with frequency  $2\omega$  as compared to the DC terms  $\mathbf{d}^{(\pm)} \cdot \mathbf{E}^{(\mp)}$  and can be dropped in the time average (which is implicit in the substitution for intensity that immediately follows below). This, along with the fact that  $V_{\text{dip}}$  is a real number, and the expression for the dipole moment (2.6) leads to:

$$V_{\text{dip}} = -\frac{1}{2\epsilon_0 c} Re[\alpha(\omega)] I(\mathbf{r}) \quad (2.10)$$

noting that the intensity is given by  $I(\mathbf{r}) = 2\epsilon_0 c |E^{(+)}|^2$ .

This is an important result describing trapping in optical dipole traps. It states that the force resulting from this potential is proportional to the gradient of the intensity, and acts to trap the atoms in a potential well. In the case of a focused laser beam (discussed later) the potential is shown graphically in [Fig. 2.1].

### 2.1.3 Scattering Rate

The process described above illustrates how the oscillating dipole induced a dipole potential which creates a trapping force. The oscillating dipole also produces dipole radiation, which accounts for the dampening term contained in the equation of motion (2.2). The Larmor formula [9] describes the total power radiated by a moving charge:

$$P_{\text{rad}}(\mathbf{r}) = \frac{e^2 \ddot{\mathbf{x}}^2}{6\pi\epsilon_0 c^3} \quad (2.11)$$

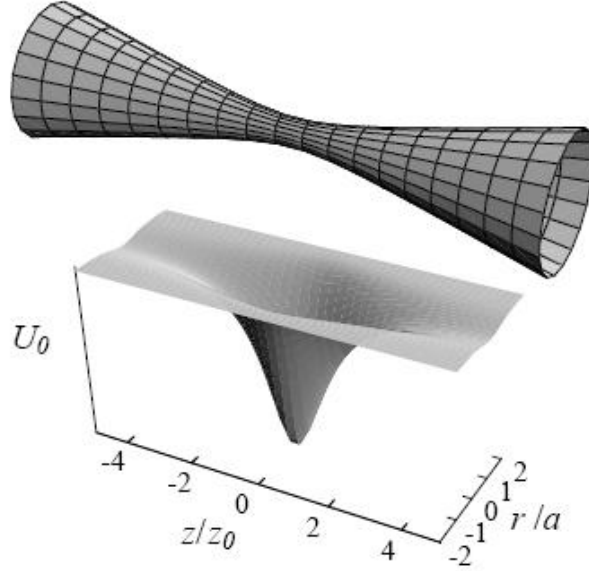


Figure 2.1: An optical dipole trap formed by a focused Gaussian laser beam. Top image shows the beam and the bottom the corresponding potential. Figure from [7].

Finding the acceleration term from (2.3) and using the imaginary part of the polarizability (2.8), the power radiated becomes

$$P_{\text{rad}}(\mathbf{r}) = \frac{\omega}{2\epsilon_0 c} \text{Im}[\alpha(\omega)] I(\mathbf{r}) \quad (2.12)$$

where the classical dampening rate [4] has been defined to be:

$$\gamma_\omega = \frac{e^2 \omega^2}{6\pi c^3 \epsilon_0 m} \quad (2.13)$$

A full derivation of the classical dampening rate can be found in [6]. The on resonance dampening rate can be further defined as:

$$\gamma_{\omega_o} \equiv \gamma = \frac{\omega_o^2}{\omega^2} \gamma_\omega \quad (2.14)$$

The power radiated by the dipole had to be initially absorbed from the incident light (photons each with energy  $\hbar\omega$ ), so the scattering rate (that is, the number of photons absorbed and emitted per unit time) can be written as:

$$\Gamma_{\text{sc}} = \frac{P_{\text{rad}}}{\hbar\omega} = \frac{1}{\hbar\epsilon_0 c} \text{Im}[\alpha(\omega)] I(\mathbf{r}) \quad (2.15)$$

#### 2.1.4 Scaling in Certain Limits

At this point, it is difficult to continue even with the classical case without taking (at the very least) a brief look at the quantum treatment of the atom. If presented with a two level system where the energy levels are separated by  $\Delta E = \hbar\omega_o$ , then at frequencies close to resonance, the

ground state atoms become strongly mixed with the excited state. Due to the decay of population from the excited state, and the emission of a photon (which is emitted randomly in all directions) the atoms undergo a random walk in momentum space leading to heating. Thus, in an effort to reduce this heating, dipole traps must be operated far off resonance. The detuning is defined as:

$$\Delta \equiv \omega - \omega_o \quad (2.16)$$

with the additional approximation that

$$|\Delta| \gg \gamma \quad (2.17)$$

Including the polarizability (2.7) and (2.8) along with the on resonance dampening rate (2.14) produces a useful expression for the dipole potential (2.10) and scattering rate (2.15) in the relevant case of large detuning:

$$V_{\text{dip}}(\mathbf{r}) = -\frac{3\pi c^2 \gamma}{2\omega_o^3} \left( \frac{1}{\omega_o - \omega} + \frac{1}{\omega_o + \omega} \right) I(\mathbf{r}) \quad (2.18)$$

$$\Gamma_{\text{sc}}(\mathbf{r}) = \frac{3\pi c^2 \gamma}{2\hbar\omega_o^3} \left( \frac{\omega}{\omega_o} \right)^3 \left( \frac{1}{\omega_o - \omega} + \frac{1}{\omega_o + \omega} \right)^2 I(\mathbf{r}) \quad (2.19)$$

To further examine the scaling of the dipole potential and the scattering rate, two limiting cases are examined:

**Rotating Wave Approximation** In this region, it is assumed that the light is far enough detuned from resonance that the approximation made above (2.17) still holds, but is close enough to one particular resonance at  $\omega_o$  such that

$$\frac{\omega}{\omega_o} \approx 1 \quad \text{and} \quad \omega_o - \omega \ll \omega_o + \omega \quad (2.20)$$

In this regime, the expression for the dipole potential (2.18) and the scattering rate (2.19) become, using (2.16):

$$V_{\text{dip}}(\mathbf{r}) = \frac{3\pi c^2 \gamma}{2\omega_o^3} \frac{\gamma}{\Delta} I(\mathbf{r}) \quad (2.21)$$

$$\Gamma_{\text{sc}} = \frac{3\pi c^2 \gamma}{2\hbar\omega_o^3} \left( \frac{\gamma}{\Delta^2} \right) I(\mathbf{r}) \quad (2.22)$$

These two equations provide very important insight into the operation of an optical dipole trap. From (2.21) it is clear that the dipole trap attracts atoms into the light field only for negative detuning. That is, the optical light must be detuned below resonance (red detuning) to create a negative trapping potential. Light tuned above the resonance frequency (blue detuning) will repel atoms. Though in the case of the work presented in this thesis, the dipole trap will be red detuned, there are some interesting blue detuned trapping techniques and applications described in [4].

Furthermore, the dipole potential scales as  $I/\Delta$  while the scattering rate (responsible for heating) scales as  $I/\Delta^2$ . Thus, in order to create the largest trapping potential with long lifetimes, the detuning must be increased while at the same time increasing the intensity of light.

**Near DC Limit** In the limit of extremely large red detuning (such is the case with CO<sub>2</sub> lasers operating at  $\lambda = 10.6\mu\text{m}$  it can be said that  $\omega \approx 0$ . In this case, the scattering rate is extremely small, resulting in trap lifetimes upwards of 300 seconds [10] and a dipole potential that scales with intensity but has no frequency dependence:

$$V_{\text{dip}} = -\frac{3\pi c^2 \gamma}{\omega_o^4} I(\mathbf{r}) \quad (2.23)$$

## 2.2 Semi-Classical Model

A more accurate description of optical dipole traps includes the complex energy level structure of atoms, along with the hyperfine structure in both the ground and excited states. We begin by considering a simple two level atom, consisting of a ground state  $|g\rangle$  and an excited state  $|e\rangle$  with an excitation frequency  $\omega_o$ .

It is crucial to note that treating a real atom (with a complex energy level structure) as a two level system requires detuning far enough from resonance such that (2.17) holds, so that the hyperfine structure of the atom cannot be distinguished. However, the incident light frequency must be close enough to a certain resonance (in this case, the one that exists at  $\omega_o$ ) to ensure we stay within this particular two level regime. This is analogous to the approximation made in (2.20) and is shown schematically in Fig. 2.2. Therefore, the results obtained from the two level approximation should match the results obtained using the rotating wave approximation in the classical case.

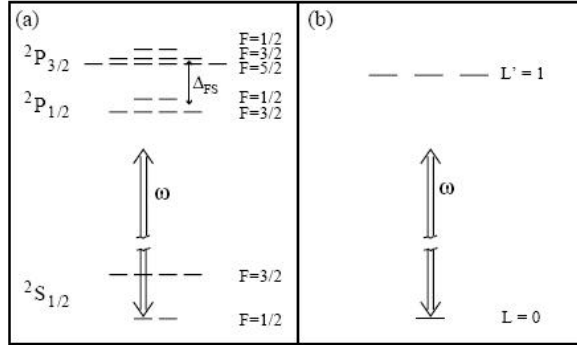


Figure 2.2: In (a) the internal states of an alkali atom are shown, with hyperfine splitting resolved. In (b) the optical detuning is such that the hyperfine splitting is unresolved, and the system simplifies to a two-level case. Figure from [7]

### 2.2.1 Decay Rate

In the classical case, the dampening co-efficient resulted from the emission of absorbed radiation induced by the oscillating dipole. In the semi-classical approach, the dampening term corresponds to the spontaneous emission rate of the atom. This is found via time dependant perturbation theory and the relationships between the Einstein A and B co-efficient [11]. For a two level system, the result is:

$$\gamma = \frac{\omega_o}{3\pi\epsilon_o\hbar c^3} |\langle e|\mu|g\rangle|^2 \quad (2.24)$$

where  $\langle e|\mu|g\rangle$  is the dipole matrix element between the ground and excited state, and  $\mu = -e\mathbf{r}$  represents the electric dipole operator [4]. The classical result is recovered (2.14) when the dipole matrix element is set to that of the quantized harmonic oscillator

$$\langle e|\mu|g\rangle = -eX_t = -e\sqrt{\frac{\hbar}{2m\omega_o}} \quad (2.25)$$

where  $X_t$  is the natural length scale for the quantized harmonic oscillator [7]. Also note that the first  $e$  in the above relation represents the excited state, while the latter  $e$ 's represent the electron charge.

### 2.2.2 Stark Shift

The effect of laser light on the energy levels of the atomic system can be treated using time-independent perturbation theory [4] [11]. The new Hamiltonian for the perturbed case is given by  $H = H^o + H_1$  where  $H_1$  is the perturbation from the unperturbed state (called the interaction Hamiltonian in this case), given by  $H_1 = -\mu\mathbf{E}$  where (again)  $\mu$  is the electric dipole operator. To first order, the shift in energy is always 0 [12]. However, second order theory gives the general result for the shift in the  $i$ -th state with unperturbed energy  $\Xi_i$  written as:

$$\Delta E_i = \sum_{j \neq i} \frac{|\langle j|\mu|i\rangle|^2}{\Xi_i - \Xi_j} \quad (2.26)$$

The energies represented by  $\Xi$  are the combined atom plus field energies [4]. For a two level system, the ground state level has zero internal energy and the light field energy is  $n\hbar\omega$ , dependent on the number of photons,  $n$ . So, the total energy of the unperturbed ground state is  $\Xi_i = (n-1)\hbar\omega + \hbar\omega_o$ . Thus,  $\Xi_i - \Xi_j = \hbar\Delta_{ij} = \hbar\Delta$  where  $\Delta$  is simply the detuning of the incident light from resonance. For the two level system, using (2.24) to substitute the dipole matrix element for the decay rate, (2.26) becomes:

$$\Delta E = \pm \frac{|\langle e|\mu|g\rangle|^2}{\hbar\Delta} |\mathbf{E}|^2 = \pm \frac{3\pi\epsilon_o c^3}{\omega_o^3} \frac{\gamma}{\Delta} |\mathbf{E}|^2 \quad (2.27)$$

The energy shift for the ground and excited states is given by the upper and lower sign (respectively). Also note the difference in the  $E$  on the LHS representing energy, and the on the RHS representing the electric field. This result is the quantum analog to the dipole potential found through the classical model. In the case at hand (with red detuning so that  $\Delta < 0$ ), atomic interactions with the light shift the ground state energy downwards. This thesis considers a far detuned case where the atom resides most of the time in ground state, with the result that the energy shift acts to attract and trap the atoms [Fig. 2.3].

Similar to the classical case, two different limiting cases can be applied to the energy shifts:

**AC Stark Shift** If the incident light is represented by an oscillating electric field, then it can be written that  $|E|^2 = \frac{I}{2\epsilon_o} c$ , and the energy shift in (2.27) becomes:

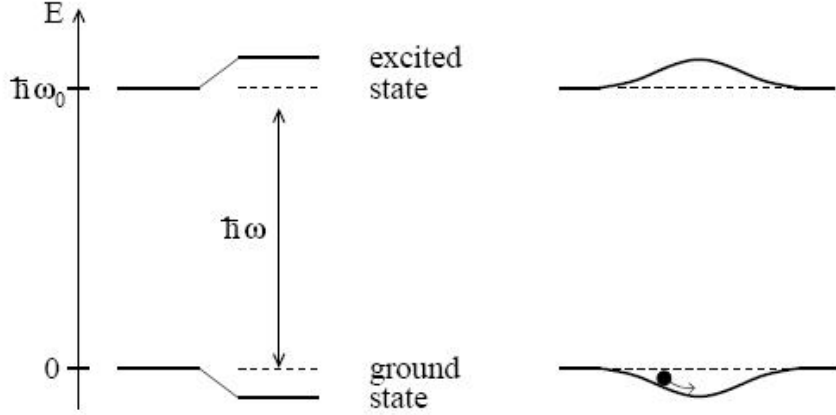


Figure 2.3: Left hand side shows the effect of red detuning shifting the ground state energy downwards. On the right hand side the effects of an inhomogeneous intensity field produced by a Gaussian laser beam is shown. Higher intensities produce a greater downward energy shift, creating a trap. Figure from [4]

$$\Delta E = \pm \frac{3\pi c^2}{2\omega_o^3} \frac{\gamma}{\Delta} I(\mathbf{r}) \quad (2.28)$$

Which is the same result as in the limit of the rotating wave approximation derived through classical methods (2.21). This is not unexpected, as the rotating wave approximation is implicit in the assumption of a two level system.

**DC Stark Shift** If it is assumed that the incident radiation is well represented by a DC electric field then, since  $|E^{AC}|^2 = |E^{DC}|^2/2$ , one can write  $|E|^2 = \frac{I}{\epsilon_o c}$  and let  $\omega \approx 0$  (DC field) to obtain the DC Stark Shift from (2.27):

$$\Delta E = \mp \frac{3\pi c^2 \gamma}{\omega_o^4} I(\mathbf{r}) \quad (2.29)$$

where, as before, the upper and lower signs represent the shift in the ground and upper states respectively. Since  $\omega \approx 0$  implies that  $\Delta < 0$ , red detuning is guaranteed. This results agrees with the classical result in the DC limit (2.23).

### 2.2.3 Multi-Level Atom

The extension of the previous results to a multi-level system requires (thankfully) only slight modification. As the assumption of the two level system has been dropped, the rotating wave approximation goes with it. First, to clean up the notation, define  $D_{mn} = \langle m | \mu | n \rangle$  to be the dipole matrix element between the  $m$  and  $n$  states of the atom. Now, the decay rate (2.24) can be extended to a multi level system [12]:

$$\gamma_{mn} = \frac{\omega_o^3}{3\pi\epsilon_o\hbar c^3} |D_{mn}|^2 \quad (2.30)$$

### 2.3. Gaussian Beam Trap

The dipole trapping potential can be calculated from the classical result (2.18), while using the quantum term for the decay rate (2.30), and summing over the energy shifts from all transitions. The quantum nature is implicit in the decay rate via the dipole matrix element, and transitions to the same energy level ( $m = n$ ) are (clearly) disallowed. Similarly, the resonance frequency must be summed over the frequencies for all transitions  $\omega_{mn}$ .

$$V_{\text{dip}} = \sum_{m \neq n} -\gamma_{mn} \cdot \frac{3\pi c^2}{2\omega_{mn}^3} \left( \frac{1}{\omega_{mn} - \omega} + \frac{1}{\omega_{mn} + \omega} \right) I(\mathbf{r}) \quad (2.31)$$

Likewise, the classical result for the scattering rate (2.19) can be modified, and summed over the contribution to the decay from all energy levels:

$$\Gamma_{\text{sc}} = \sum_{m \neq n} \gamma_{mn} \cdot \frac{3\pi c^2}{2\hbar\omega_{mn}^3} \left( \frac{\omega}{\omega_{mn}} \right)^3 \left( \frac{1}{\omega_{mn} - \omega} + \frac{1}{\omega_{mn} + \omega} \right)^2 I(\mathbf{r}) \quad (2.32)$$

The only assumption that is tied to the above equations is that the incident light is far detuned from a resonance (2.17). The laser light used in this thesis ( $\lambda = 1090$  nm) falls within this consideration. However, it is on the far edge of the rotating wave approximation, and using it may not give accurate predictions for trap depth and/or scattering. Thus, these approximations cannot be safely used. Their results, however, are still very helpful in understanding the trapping physics. Instead, (2.31) and (2.32) can (and are) used with full confidence.

## 2.3 Gaussian Beam Trap

To predict the trapping depth and trapping frequencies of an optical dipole trap, some basic information about Gaussian beams is employed, and applied to the dipole potential (2.31). The intensity of a Gaussian beam [Fig 2.4] can be written as

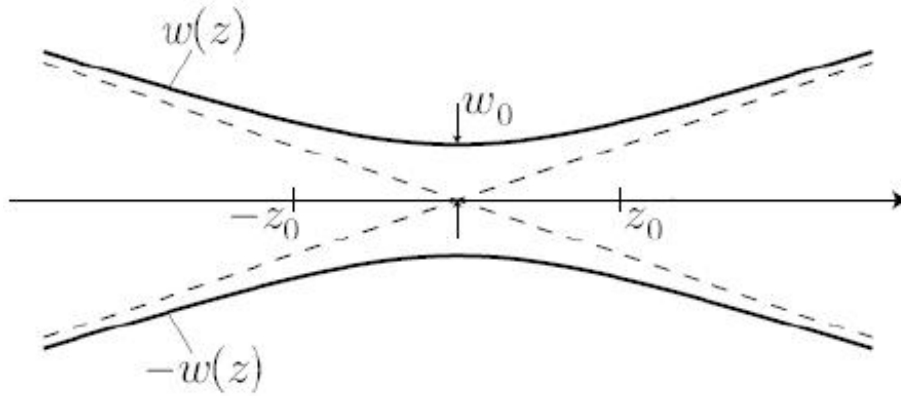


Figure 2.4: Schematic of a Gaussian beam profile. Figure from [12]

$$I(r, z) = \frac{2P}{\pi w^2(z)} \cdot e^{-\frac{2r^2}{w^2(z)}} \quad (2.33)$$

with

### 2.3. Gaussian Beam Trap

---

$$w(z) = w_o \sqrt{1 + \left(\frac{z}{z_o}\right)^2} \quad (2.34)$$

where  $P$  is the total power, and  $z_o$  is the Raleigh range, given by:

$$z_o = \frac{w_o^2 \pi}{\lambda} \quad (2.35)$$

Using this form of the intensity in (2.31) gives:

$$V_{\text{dip}}(r, z) = V_o \left(\frac{w_o}{w(z)}\right)^2 \cdot e^{-\frac{2r^2}{w^2(z)}} \quad (2.36)$$

where  $V_o$  is the trap depth, given by (2.31) and (2.33) with  $r = z = 0$ :

$$V_{\text{dip}} = \sum_{m \neq n} -\gamma_{mn} \cdot \frac{3\pi c^2}{2\omega_{mn}^3} \left(\frac{1}{\omega_{mn} - \omega} + \frac{1}{\omega_{mn} + \omega}\right) \frac{2P}{\pi w^2} \quad (2.37)$$

When atoms are at a temperature  $T \ll V_o$  they are concentrated near the focus of the beam at the center of the trap, and see a potential that can be approximated as harmonic. Taking  $\frac{z}{z_o} \ll 1$  and  $\frac{r}{w} \ll 1$  and using the form for  $w(z)$  from (2.34), the trap potential becomes

$$V(r, z) \approx -V_o \left[1 - 2\left(\frac{r}{w_o}\right) - \frac{z}{z_o}\right] = -V_o + \frac{1}{2}m\omega_r^2 r^2 + \frac{1}{2}m\omega_z^2 z^2 \quad (2.38)$$

comparing the two equations gives the trapping frequencies for the radial and axial directions:

$$\omega_r = \sqrt{\frac{4V_o}{mw_o^2}} \quad (2.39)$$

$$\omega_z = \sqrt{\frac{2V_o}{mz_o^2}} \quad (2.40)$$

A comparison of the theoretical trap frequencies from calculations to those found from experiment can act as a gauge of the quality of the beam at the focus, and give information about its power and waist size at that point.

**Parametric Excitation** If the optical dipole trap is modelled as a harmonic potential well, a trapped atom can be thought of as oscillating from side to side in trap, which gives rise to the frequencies defined in (2.39) and (2.40) above. These oscillation, in classical terms, can be modelled by [16]:

$$\ddot{x} + \beta(t)(\dot{x}) + \omega^2(t)x = 0 \quad (2.41)$$

where  $\beta(t)$  and  $\omega(t)$  are the time-dependant damping coefficient and natural frequency of the oscillator, respectively. Applying a force to modulate the natural frequency of the system, with amplitude  $f_o$  and frequency of modulation  $\omega_m$  has the effect of changing the natural frequency to the form:

$$\omega^2(t) = \omega_o^2(1 + f_o \sin(\omega_m t)) \quad (2.42)$$

Clearly, there is a maximum amplification in the oscillation when  $\sin(\omega_m t) = 1$ , which occurs when  $\omega_m = 2\omega_o$  or at any sub harmonic. This condition arises from the need to force the oscillation as the atom (classically speaking) reached its maximum amplitude; If the atom is forced every time it reaches this point, the forcing function will need to have twice the oscillation frequency. If this forcing only occurs every second time, the forcing function will need to have a frequency equal to the oscillation frequency. This continues for all sub-harmonics, but does not apply for frequencies greater than twice the oscillation frequency because the forcing function will not act on the atom at its maximum amplitude. The width of the resonance, for the case when  $f_o \ll 1$  is given by [16]:

$$\Delta\omega = \omega_o \cdot \left(1 + \frac{1}{2} \cdot f_o\right) - \omega_o \left(1 - \frac{1}{2} \cdot f_o\right) = f_o \cdot \omega_o \quad (2.43)$$

In an optical dipole trap, the modulating force is provided by varying the power of the trapping beam at a set frequency. In this context, maximum amplification of the oscillation implies an increase in energy of the trapped atoms, which manifests itself as an observable decrease in the number of trapped atoms. By varying the modulation frequency of the trapping beam over a range of frequencies, the radial and longitudinal trapping frequencies (derived theoretically above) can be confirmed.

# Chapter 3

## Laser Characterization

The optical dipole trap in this thesis was built using a SPI 100W fibre laser. What follows is a characterization of the laser properties, and effects on the experimental setup.

### 3.1 Calibration

The laser is rated to 100W however, the effective power after passing through the optical isolator and reflecting off an AR coated mirror (mounted to the legs of the optical isolator mount) will be lower. The power at this point is defined as the effective power of the laser, and is the basis of the input voltage to output power calibration. The relationship between the input voltage, actual and effective output power [Fig. 3.1] is generally linear, with a relationship between the voltage and effective power defined by:

$$P = 10.772 \cdot V - 10.5468 \quad [\text{W}] \quad (3.1)$$

where  $P$  is the effective output power and  $V$  is the input voltage in volts. This relationship is used to define the voltage sent to the laser control when a power is set using the `spi_control` python command. The power absorbed by the optical isolator is 3.3% and is independent of the output power.

### 3.2 Power Spectrum

A spectrum analyser was used to examine the spectral power of the laser at various output power settings around the expected peak of 1090nm [Fig 3.2]. At low powers, there is a distinct and relatively narrow peak near 1091nm. The peak widens and broadens with movement towards higher output powers, but produces a clean signal with no secondary peaks. The drift of the peak spans a range of 0.5nm, moving from 1091.4nm at 5W to 1090.9nm at 100W. On average, the peak spectral power occurs at 1091.1nm, with a width exceeding 1nm.

### 3.3 Power Fluctuations

The SPI trapping laser is said to be randomly polarized, which initiated an attempt to measure (if they existed at all) the frequency and amplitude of the polarization changes as it related the output power of the beam. An understanding of the overall power fluctuations are important in determining trapping parameters, as well determining possible trap depths where the power modulation could create unintended parametric heating within the trap. Likewise, in the cross beam trap setup, when light hits the MOT cell at an angle the two different polarizations will have different transmission co-efficient. If these fluctuations are large, there could be a marked

### 3.3. Power Fluctuations

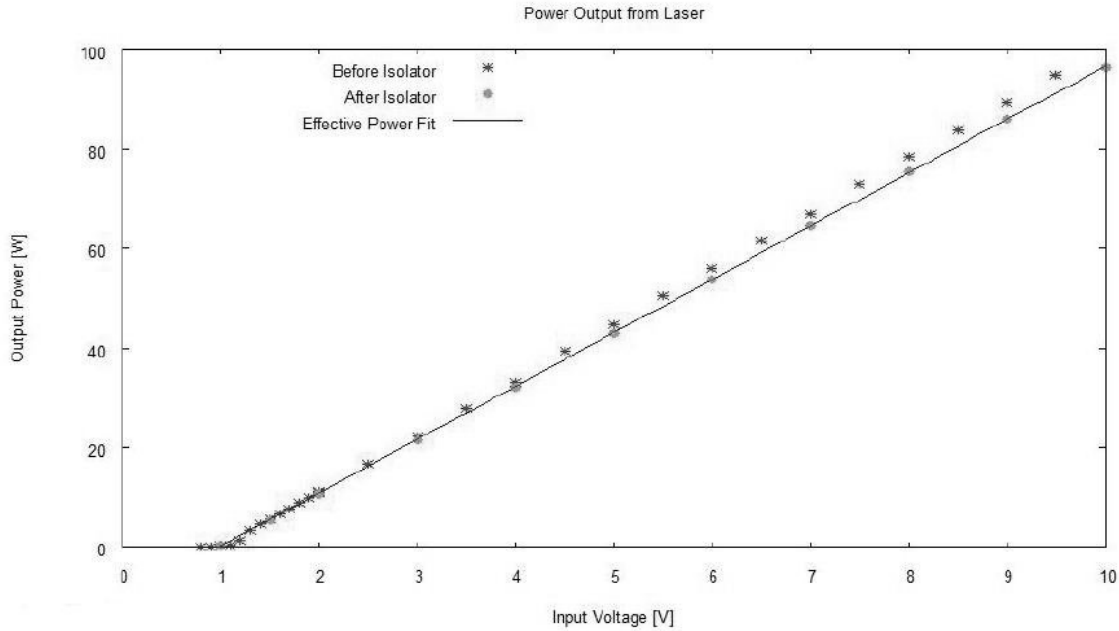


Figure 3.1: Output power before (stars) and after (dots) of laser vs. applied input voltage. Also shown is the fit (3.1) to the effective power (measured after going through optical isolator and a single reflection of an AR coated mirror).

difference between the trapping arms, and on the effectiveness of the trap.

A single Glan-Thompson polarizer was used to separate the light into its S and P polarization components (in this instance, horizontal and perpendicular to the optical table). The two polarized beams were each then sent through another Glan-Thompson rotated nearly perpendicular to the first, such that it acted as an attenuator, and finally onto two photo detectors. The response of the photodiodes was measured in order to convert the output mV readings on the oscilloscope to power readings of the incident light. However, because the amount of attenuation provided by the Glan-Thompsons was not consistent between the two different polarization beams, the relative power of the two arms contains little useful information. It is noted that measurements of the power in both arms (after the initial polarization splitting) showed nearly equal powers, with the accuracy of the setup.

By viewing the power (as seen on an oscilloscope) as a function of time, any trends in the power fluctuations can be seen. In phase fluctuations between the two readings correspond to overall power fluctuations, and out of phase fluctuations correspond to power oscillations due to the changing polarization. In and out of phase changes can be extracted from the oscilloscope measurements by adding or subtracting (respectively) the two power readings. Unfortunately, there was quite a bit of noise associated with the two photo detectors, which acted to hide some of the smaller oscillations. Readings taken with no incident light [Fig 3.3] show noise oscillations at frequencies of 13MHz and 3Mhz, which must be taken into consideration when looking for in and out of phase oscillations of the laser light.

### 3.3. Power Fluctuations

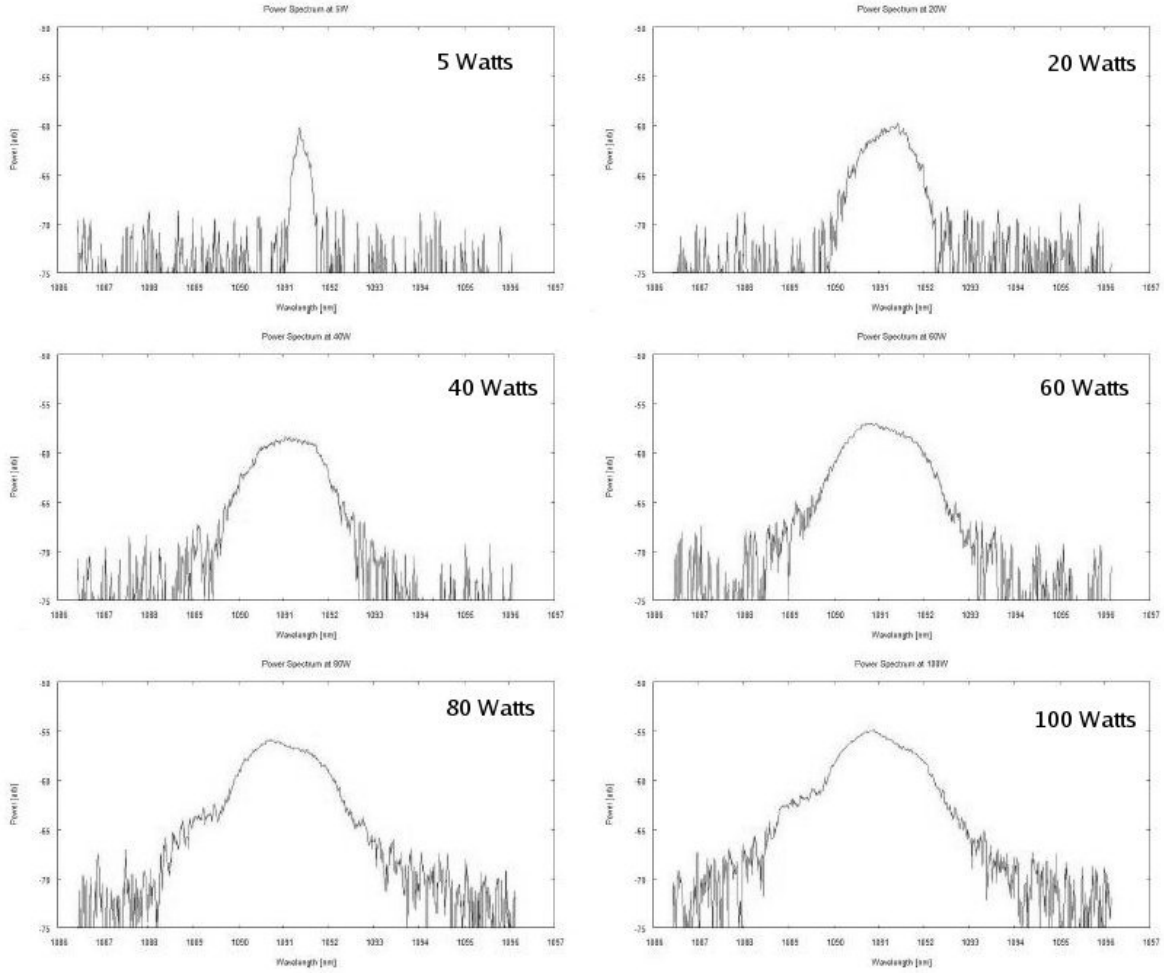


Figure 3.2: Power spectrum of SPI laser at varying powers. From left to right by row, starting at top left: 5W, 20W, 40W, 60W, 80W, 100W.

#### 3.3.1 In Phase Oscillations

In phase (overall power fluctuations) were found at frequencies of 210kHz [Fig. 3.4] and 30Hz [Fig. 3.5]. The slow fluctuations (30Hz) were much stronger than the faster (210kHz) oscillations, with amplitudes of 2.6% of the total power for the former, compared to 0.7% for the latter (after accounting for the background noise). In both figures, the top image shows the individual power readings for the two different polarized beams, and the bottom image shows the added (out of phase, dark plot) and subtracted (in phase, light plot) oscillations.

#### 3.3.2 Out of Phase Oscillations

Although some small polarization (out of phase) power fluctuations can be seen in Figure 3.4, more prominent oscillations were found at different time scales. At low powers (measurement taken at 1.4W), oscillations amplitudes as high as 3.4% were seen, with a frequency of 910Hz [Fig 3.6]. However, with increasing powers, the fluctuations decreased until they are hidden beneath

### 3.4. Relaxation Oscillations

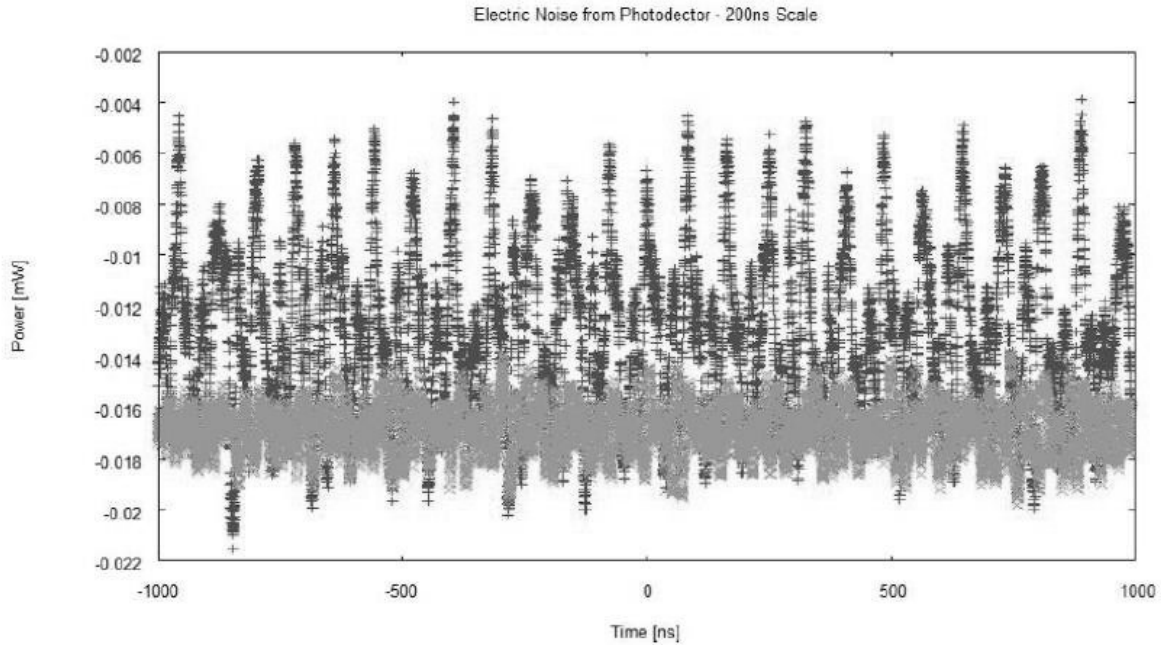


Figure 3.3: Fluctuations due to noise from photo detectors. Readings taken with laser off, but detectors unblocked in order to account for background light. Notice oscillations at 13Mhz and 3Mhz.

the noise the photo detectors (above 5W - data shown taken at 30W) and cannot be distinguished [Fig 3.7]

### 3.4 Relaxation Oscillations

Relaxations oscillations occurred when the laser is initially modulated on, at a frequency on the order of 20Mhz. The delay between the time the voltage signal is sent to turn on the laser and the start of the oscillations varies inversely with the power setting. Though the laser documentation claims powers of up to 20x the set point power can occur during the relaxation oscillations, the maximum observed on the oscilloscope data was on the order of 5x. In order to reduce the power of light that hit the cell, a short turn on python command was written that (independent of the final set point power) turned on the laser to 2W, and at the completion of the corresponding relaxation oscillations, set the power to the final set-point value. The choice of 2W gave a good compromise between the highest oscillation power (less then 10W) and turn on time. Again, independent of the final power setting, the laser is turned on to any given power within a time of  $400\mu\text{s}$ . The time evolution of the laser output power before and after correction for the oscillation is shown in Figure 3.8. There is also a short delay of  $15\mu\text{s}$  between the modulate off signal, and the time the output power is fully off.

### 3.4. Relaxation Oscillations

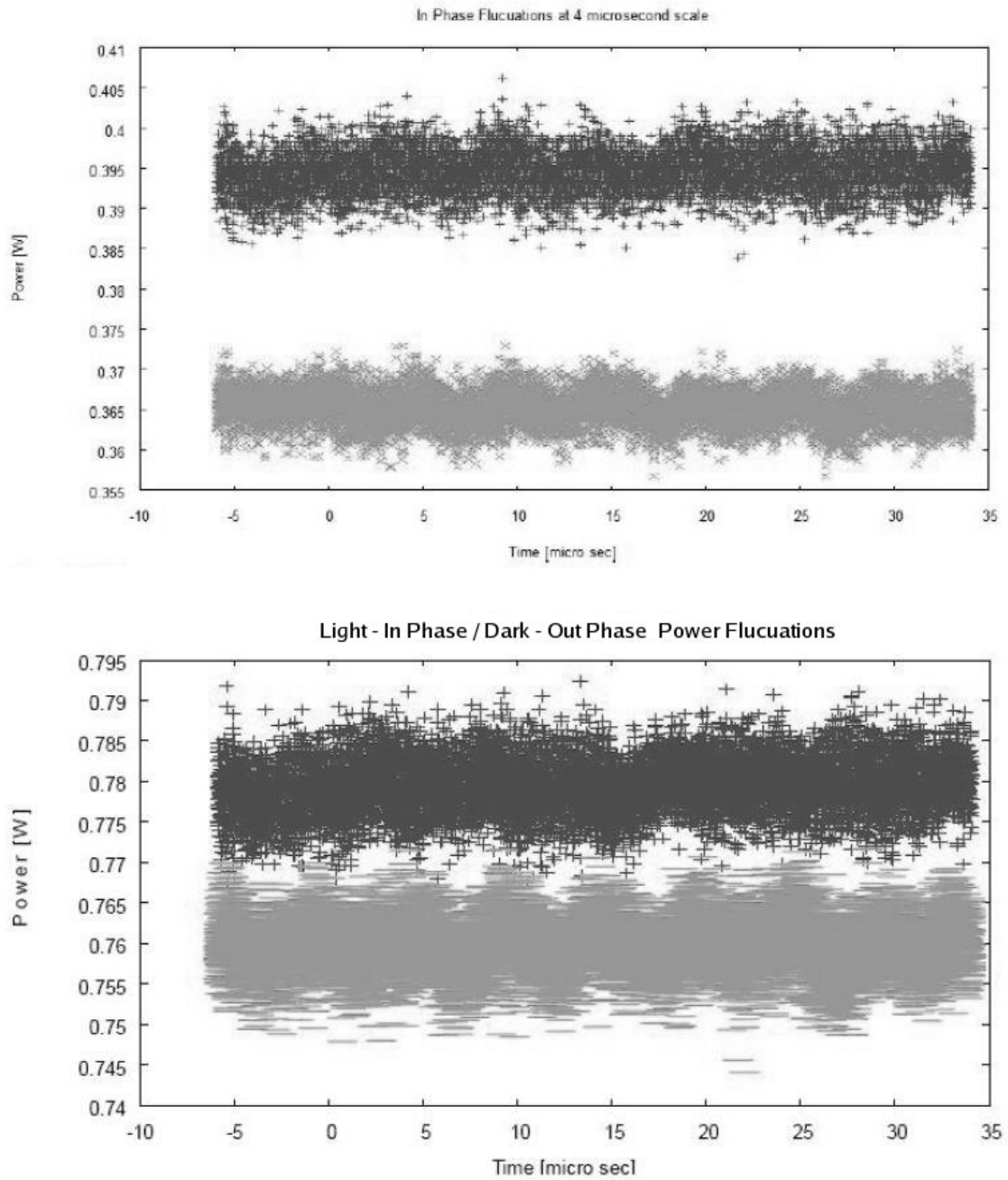


Figure 3.4: Fast in phase fluctuations at 210kHz. Top plot shows individual detector readings, and the bottom plot shows the added (dark) and subtracted (light) readings. Note the sinusoidal fluctuations in the light (in phase) reading. Also note there is a small amount of out of phase (dark) component

### 3.5. Beam Distortion

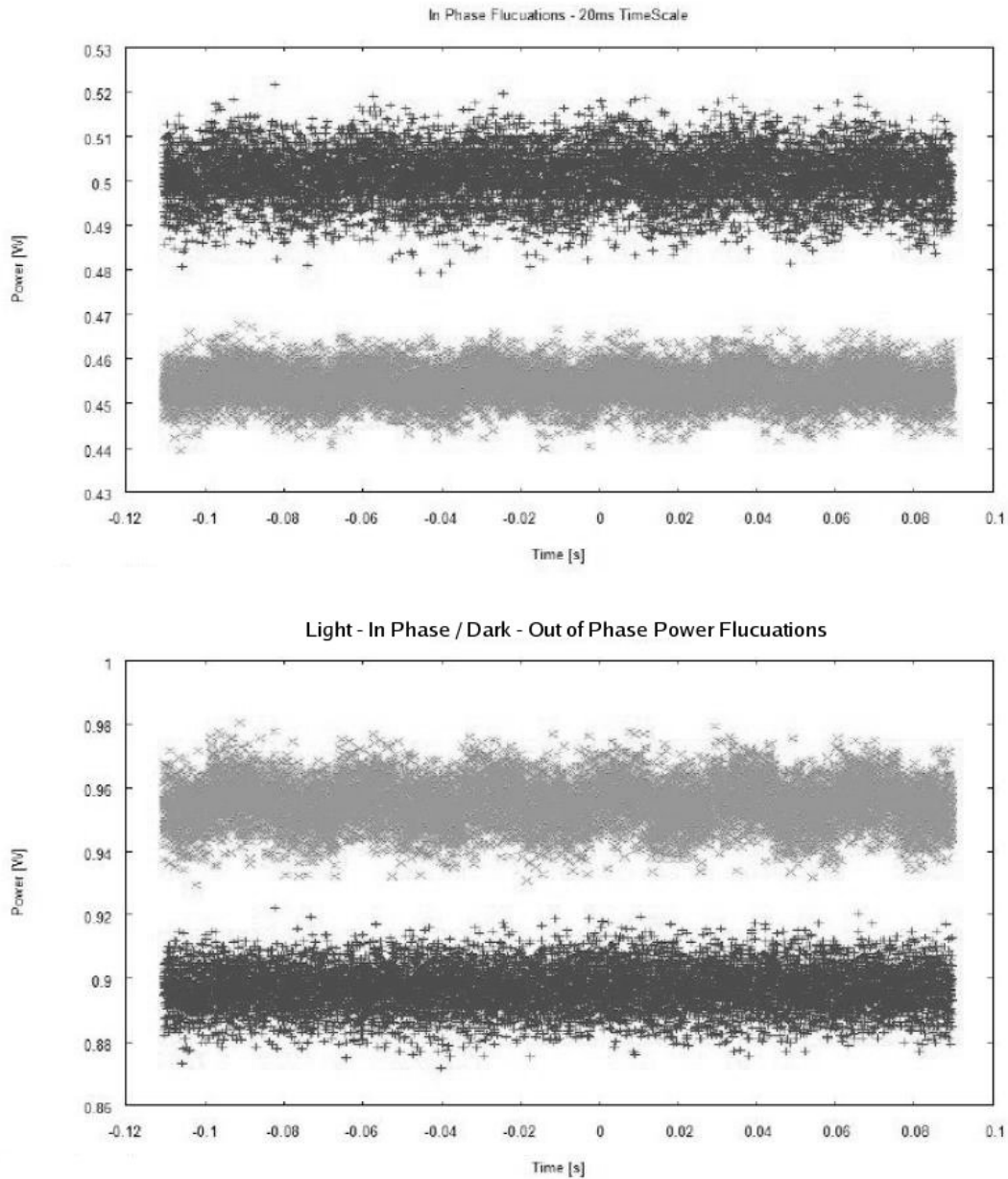


Figure 3.5: Slow in phase fluctuations at 30Hz. Top plot shows individual detector readings, and the bottom plot shows the added (dark) and subtracted (light) readings. At this time scale, the out of phase component is nearly constant.

### 3.5 Beam Distortion

Initial testing of the effect of high powers of light through glass flats were done on unknown type, but presumed to be BK7. No obvious effects were seen at powers up to 100W. Testing a on Pyrex flat produced obvious distortion of the beam, even at low powers ( $< 10W$ ), prompting a more

### 3.5. Beam Distortion

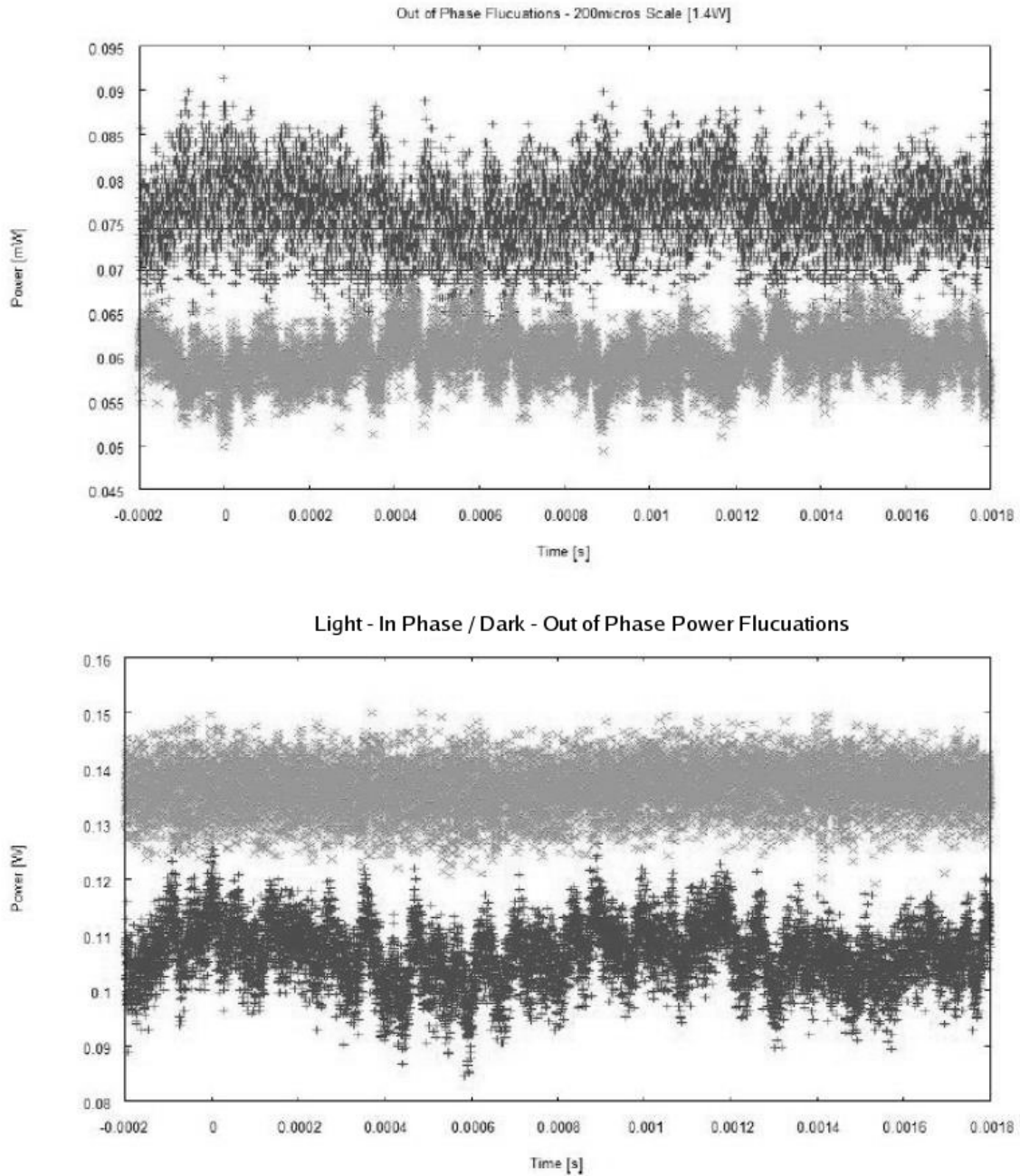


Figure 3.6: Out of phase power fluctuations at a timescale of 200ms, frequency of 910Hz. Top plot shows individual photo detector readings, and the bottom plot shows the added (dark) and subtracted (light) readings. Note the large variations in the dark (out of phase) reading.

detailed investigation of the effects of the MOT cell on the beam. A spare MOT cell, similar in size and glass makeup to the experimental cell was used. In order to image the beam and

### 3.5. Beam Distortion

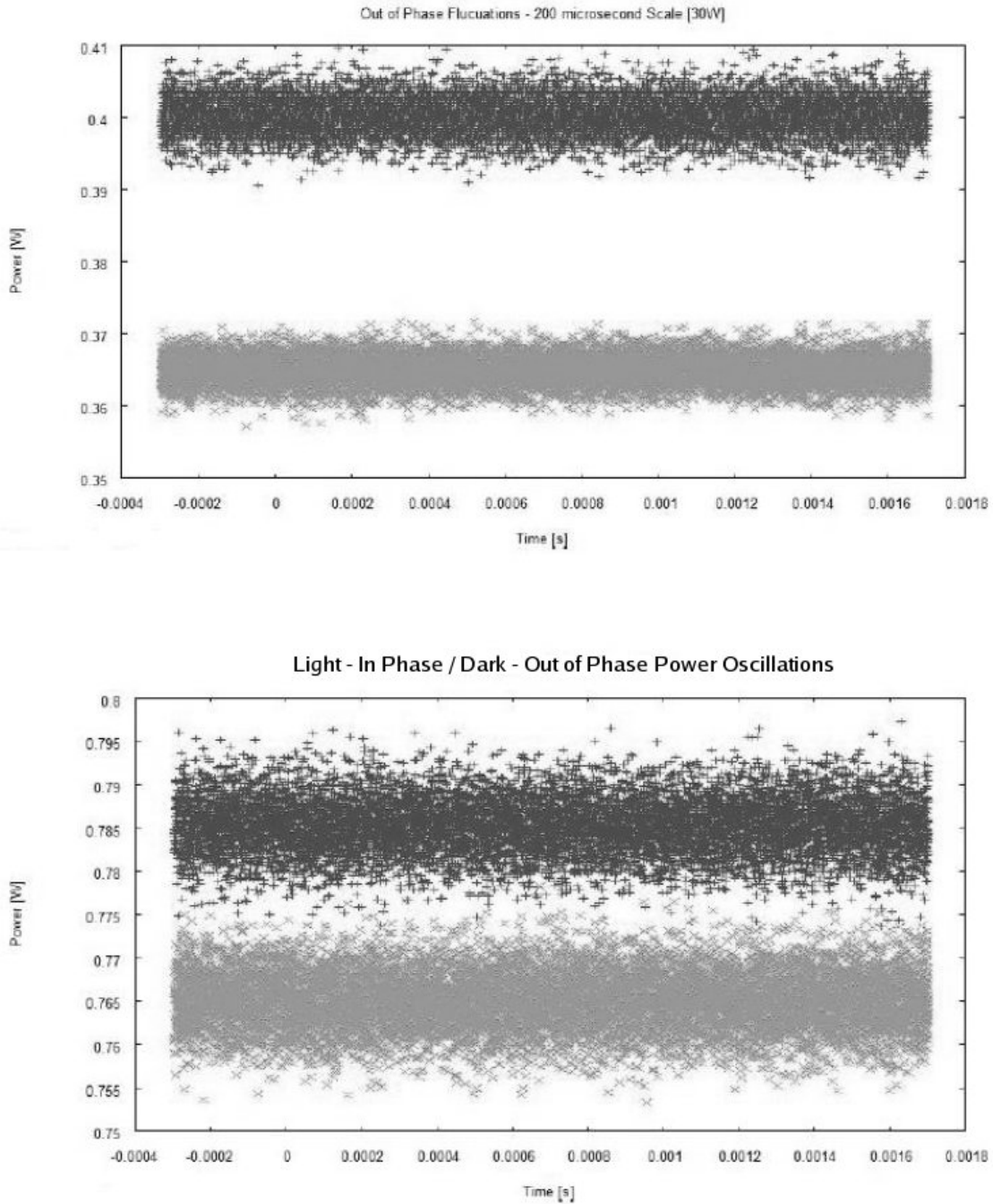


Figure 3.7: Out of phase power fluctuations at a timescale of 200ms. Top plot shows individual photo detector readings, and the bottom plot shows the added (dark) and subtracted (light) readings. When compared to the fluctuations at low powers [Fig. 3.6] the fluctuations appear completely hidden beneath the noise.

### 3.5. Beam Distortion

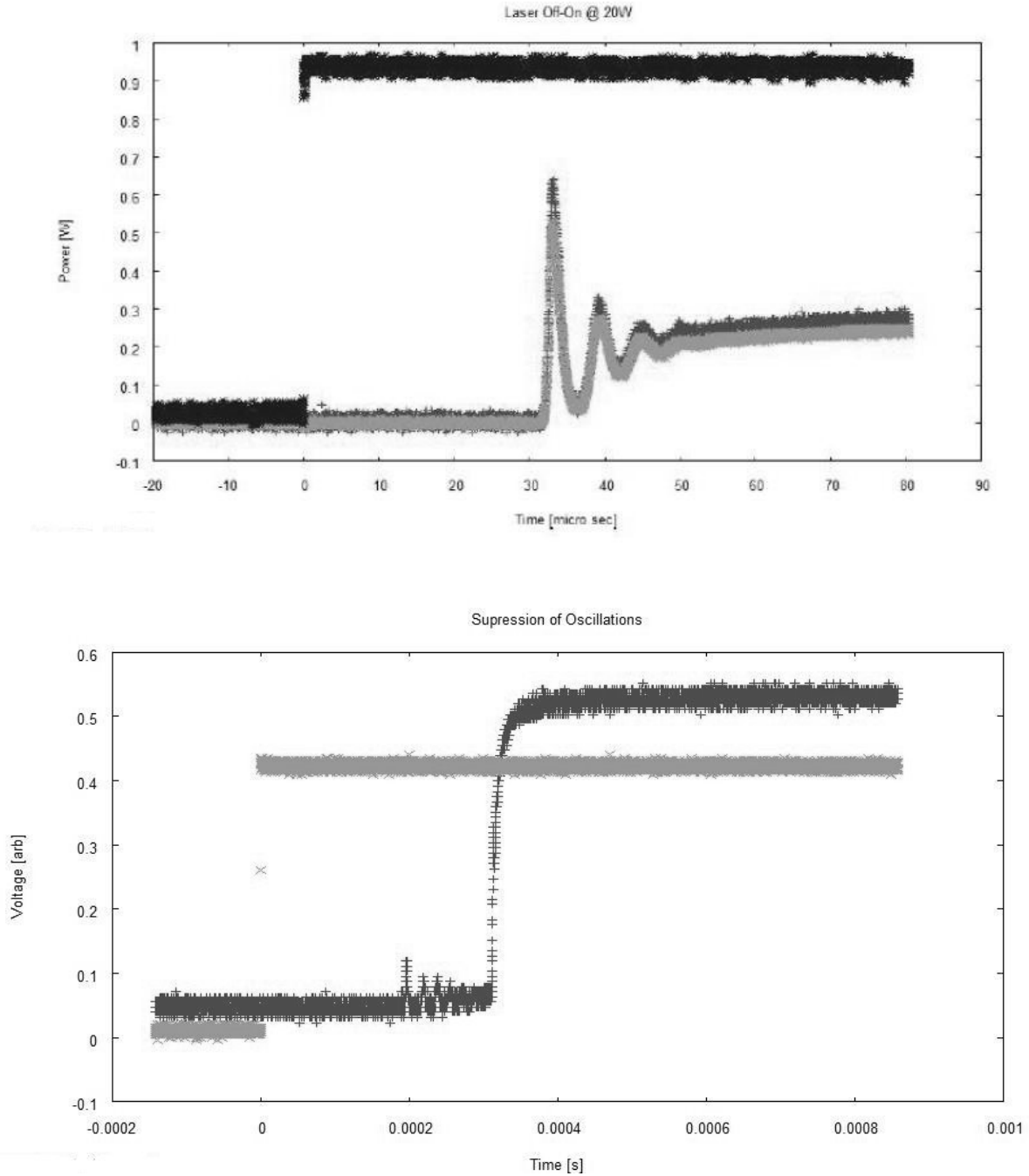


Figure 3.8: Plot of (top) relaxation oscillations when the laser is modulated on and (bottom) suppressed relaxation oscillations by modulating to small power, and then increasing to the final set point power. Note that the modulate trigger is inserted as a reference only - the relative height is unimportant.

compare it to the unobstructed beam (with no cell in place) at high powers, an optical system was set up to attenuate the beam to low enough powers as not to saturate the Sony CCD camera

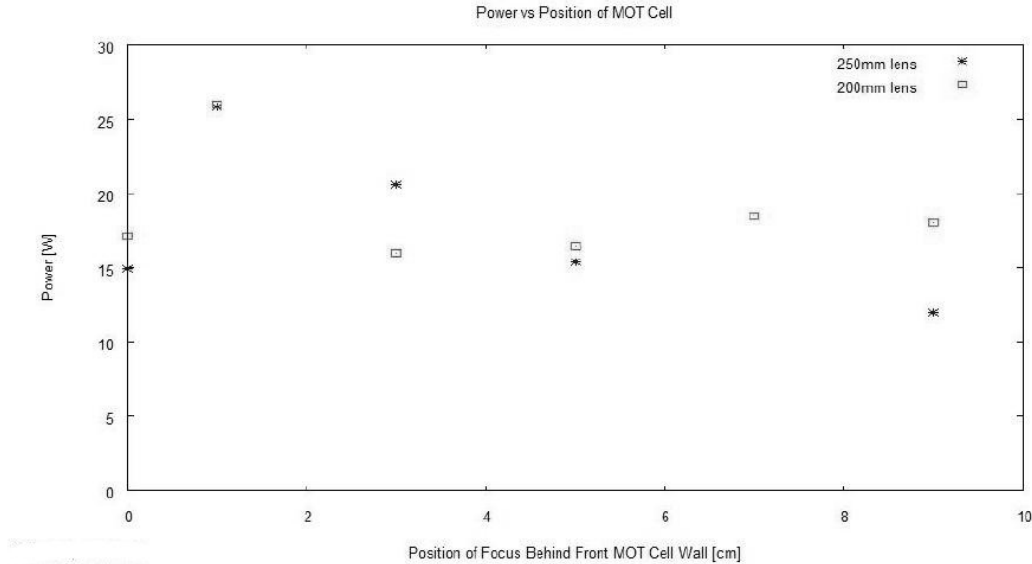


Figure 3.9: Power at which the beam appears to be distorted as imaged on the Sony CCD camera, for both a 250mm (stars) and 200mm (squares) lens. The threshold of interest where the focus is in the middle of the MOT cell (a position of 1cm on the plot) is around 26W

(or melt the neutral density filters placed before the camera to further reduce the intensity of light). The setup consisted of reflecting the beam off a glass slab (to initially cut down the power) and focusing the reflected beam through two Glan Thompsons polarisers oriented perpendicular to one another such that the combination acted as an attenuator. Finally, the beam was passed through multiple neutral density filters, and was imaged on the camera.

The beam distortion becomes noticeable at a certain threshold value, which was dependant on the relative position of the focus with regard to the MOT cell walls. The threshold power value decreased as the size of the beam hitting the cell increased [Fig. 3.9]. Because the beam had to pass through both cell walls, the beam was at its smallest at both walls when the focus was in the middle of the cell, which corresponded to the highest threshold value. The similarity in threshold power when the focus is in the middle of the cell, even though the focus is of a different size, arises from the fact that the waist size 1cm from the focus (where the light passes through the cell) are very similar, at  $132\mu\text{m}$  and  $109\mu\text{m}$  for the 200mm and 250mm lens respectively. Given this initial data, it would appear there is an upper threshold of 26W in the expected experimental setup where the beam focus is located in the center of the cell.

### 3.6 Cell Absorption and Reflection

Once it was realized that the MOT cell absorbed some power due to heat (causing expansion and the thermal lensing effects) the amount of power absorbed and reflected by the cell was examined. Specifically of interest was to check the absorption at different powers (and note any variation). In order to be sure the data was not influenced by the length of time the cell was absorbing the incident light energy, the data sets were taken moving both from high to low power and from low power to high power. No differences between the sets were seen, which is consistent with the

time dependant images (discussed below). Note that the power loss included absorption (of both cell walls) as well as reflections off of four surfaces. The power remaining after passing through the cell appeared constant over a wide range of powers, giving a transmission of 83.8%. If the assumption that equal power is lost at each cell wall holds true, the power at the center of the MOT will be roughly 91.5% of the incident power.

### 3.7 Detailed Image Analysis

The point of greatest interest is when the focus is in the middle of the MOT cell and all further discussion revolves around this setup. In order to initially classify a threshold power, the point at which beam distortion occurred was taken to be a judgement call based on the image of the beam passing through the cell as compared to the clean (no cell) beam. The change from good to bad did not occur rapidly, and there was a range over which the beam could be considered OK, but not perfect [Fig 3.10].

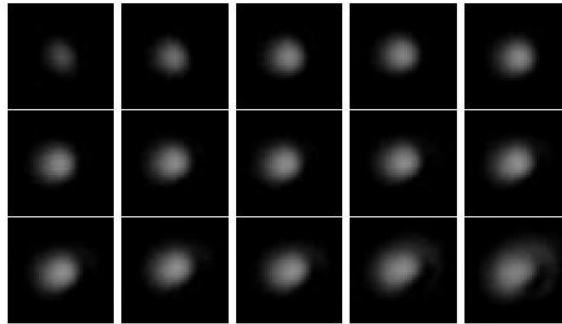


Figure 3.10: Image of beam through MOT cell with varying power. The power of the beam is, from left to right: (Top Row) 10W, 15W, 20W, 21W, 22W, (Middle Row) 23W, 24W, 25W, 26W, 27W, (Bottom Row) 28W, 29W, 30W, 35W, 40W. Note the slow progression from a 'good' beam to a 'bad' beam

In order to accurately quantify the quality of the beam after propagation through the MOT cell, versus a clean beam, the image of the beam with and without the cell were subtracted. By subtracting the clean image from the distorted, the new image showed only the distortion that occurred, but not the decrease in power from absorption (and reflection) by the MOT cell [Fig 3.11].

Ideally, if the beams were identical, the subtracted image would be dark. However, even at low powers, the subtracted image appears to have some non-zero pixel count. This could be from a number of sources, most likely associated with an increase in spot size or slight astigmatism due to passing through the glass cell at slight angle. At higher powers, the larger pixel counts are due (in part) to the distortion of the beam. To quantify the effect of the cell, the individual pixel counts were summed (giving a measure of total distortion) and plotted as a function of power [Fig. 3.12]. A baseline value of roughly 1000 counts is observed. Above powers of 25W, the total pixel count increased rapidly away from the baseline. This confirms the original estimate that the distortion threshold value is on the order of 25W.

In addition to testing at different power settings, the distortions response to time [Fig. 3.13] and angle was measured. There appears to be no variation of the distortion on long time scales

### 3.7. Detailed Image Analysis



Figure 3.11: Subtracted images of beam at varying power. From left to right, top row to bottom row: 10W, 15W, 20-30W (at 1W increments), 35W, 40W.

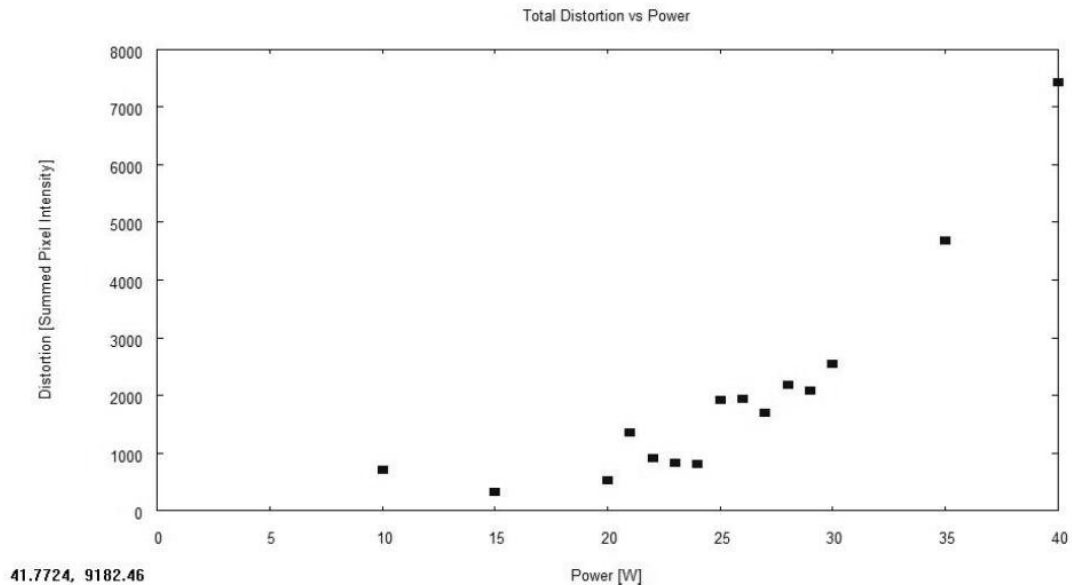


Figure 3.12: Total distortion, as measured by a sum of the individual image pixel intensities as a function of power. Focus is located at the center of the MOT cell.

(up to 5 minutes) however, the distortion does take some (undetermined, but on the order of tenths of seconds) to appear. No additional noticeable distortion appears with increasing angle (away from the perpendicular incidence).

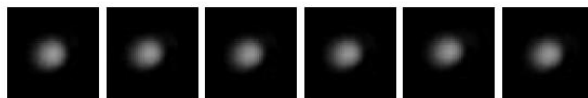


Figure 3.13: Response of the beam distortion to time, at 25W passing through a 200mm lens. From left to right: 0min, 1min, 2min, 3min, 4min, 5min.

### 3.8 Other Materials

In addition to testing the spare MOT cell, flats of other various materials were tested for comparison. Two viewports (quartz and a standard Corning 7056 glass) from a vacuum cell made by Thermionic Inc. - model numbers **QPV-150** and **ZPV-150** respectively, as well as a 4mm thick quartz slab were tested. All showed no distortion at any power, or distance from the focus. Figure 3.14 shows the images (and baseline reference of the clean beam) for the 4mm quartz slab. Finally, there was no distortion seen on any of the materials when the beam was incident at a 45 degree angle.

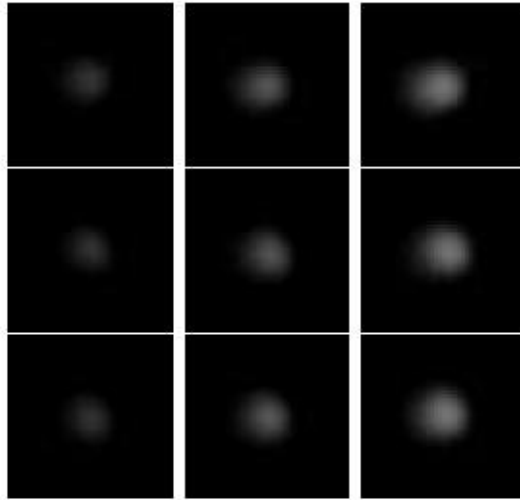


Figure 3.14: Effect of a 4mm quartz slab on the beam. All rows show, from left to right, 44W, 65W, 100W. Top row shows the unobstructed beam for comparison. Middle row shows the beam hitting the slab at the focus, and the bottom row shows the slab 10cm in front of the beam focus.

### 3.9 Cell Damage

Unfourtunately, early in the setup of the trap, damage was seen on the cell. The net effect was to focus the absorption beam, giving rise to a bright spot in the raw absorption image [Fig. 3.15]. However, this spot could not be replicated and has not been seen at other locations on the cell, implying that there may have been something on the cell to accelerate the damage in that location. However, it is possible to further damage a small area around the central location of the damage, so care must be taken when re-aligning the trap to avoid it.

### 3.10 Calculations

Given that the distortion of the beam causes an upper limit to be placed on power, but below that threshold the beam appears to be relatively unaffected, the following is the expected trap depth and trap frequencies over a range of laser output powers. The possible trap geometries with and without a beam expander are given in Table 3.1. The calculations are preformed assuming

### 3.10. Calculations

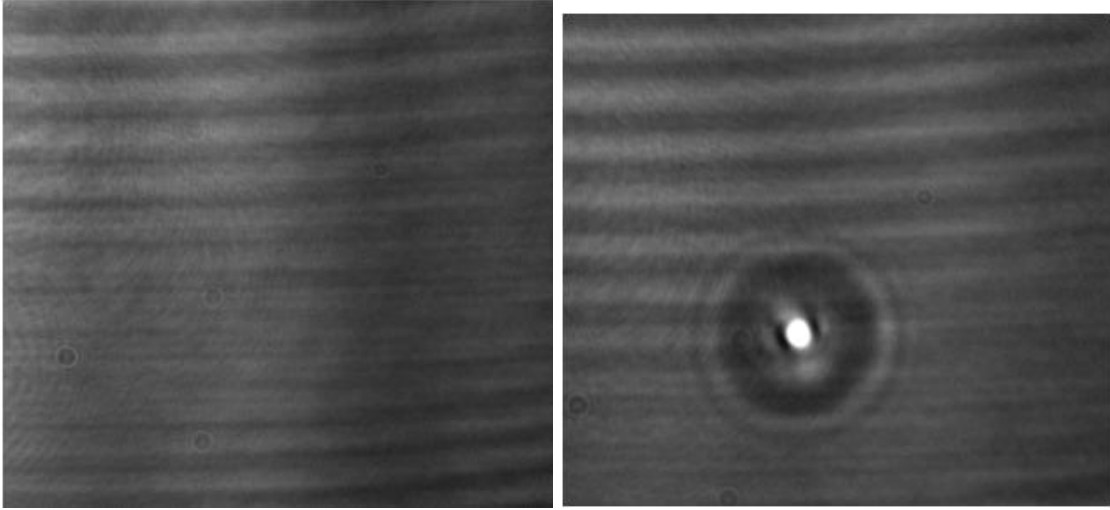


Figure 3.15: Damage to cell as seen on the absorption image (left) before and (right) after use if SPI Laser.

a power loss of 8.5% at the cell and the larger of the beam waists (without expander) for  $^{85}\text{Rb}$  [Table 3.2]. The powers used were chosen based off the powers used in testing for the radial trap frequencies (8.5W and 34W), all other parameters (15W, 30W) and the max power of the trap (40W). In addition, the calculations for axial trap frequency are only valid for the single arm traps. Full details on the calculations can be found in Appendix C.

	Predicted [ $\mu\text{m}$ ]	(4/3) Prediction [ $\mu\text{m}$ ]	Measured [ $\mu\text{m}$ ]
With Expander	13.3	17.7	22.7
No Expander	26.7	35.6	37.7

Table 3.1: Predicted and Measured values for beam focus using 200mm lens

Power [W]	Trap Depth [mK]	Radial Freq. [kHz]	Axial Freq. [Hz]
8.5	0.56	1.9	12.9
15	1.0	2.6	17.1
30	2.0	3.6	24.3
34	2.3	3.9	25.8
40	2.7	4.3	28.0

Table 3.2: Trap Depth and Frequency calculations for  $^{85}\text{Rb}$

# Chapter 4

## Experimental Setup

### 4.1 Cross Beam Trap Design

Due to the possibility of damage on the cell, the final setup required the trapping light be split into two separate beams, crossing at their focus at the center of the trap, creating a cross beam trap. This allows for the use of up the 40W of power (20W through each arm) and also provides a more localized trap potential due to the small area of intersection of the two beams. All the optics used in the setup are AR-coated for near IR light, and are considered high power optics, able to handle intensities up to  $1\text{MW}/\text{cm}^2$ .

The laser itself is run off of a control box created by Janelle van Dongen, and can be controlled manually or via inputs from analog and digital outputs. To operate, the laser requires a 5V input that can be used to modulate the laser on and off at fast frequencies, an input voltage that determines the output power, and its internal interlock to be disabled (achieved through a key on the back of the housing box, a switch on the control box, and ensuring the emergency stop button is not pushed in). Finally, 2.5 LPM of water at  $20^\circ\text{C}$  are required to operate the laser, and it has a built in switch that will disable the laser if there is a lower flow rate, or if the water temperature drops below  $15^\circ\text{C}$ .

The laser output is sent through an optical isolator (provided by the manufacture) which is secured to a mount designed and built in the UBC student machine shop. Also attached to the mount is a two inch diameter mirror purchased from CVI (part number **Y1-2025-45-P**) which directs the beam perpendicular to the table. After being split via a 50/50 beam splitter<sup>1</sup> (part number **BS1-1090-50-2025-45UNP**), coated for unpolarized light with a  $45^\circ$  angle of incidence, the first arm is reflected off of another two inch mirror and passed through a 200mm lens (part number **PLCX-38.1-103.0-C-1064**) while the second arm passes through another 200mm lens (part number **PLCX-38.1-103.0-UV-1064**) directly after the beam splitter. The lens are made of different material (BK7 and Fused Silica respectively) and have widely different focal positions of 23cm and 20cm from the cell center (indicating, perhaps, a varying focal length, which was confirmed in the characterization of the trap, below). The beams are captured by two separate beam dumps after passing through the cell. The beam dump for the first arm is water cooled, and capable of handling 100W for at least 10 minutes. The beam dump for the second arm is not water cooled, and is capable of handling 30W for up to 5 minutes before becoming too hot to handle.

---

<sup>1</sup>After the trap was aligned, the power reflected and transmitted was tested, and in this configuration, the incident light is split equally.

## 4.2 Imaging

A full explanation of the imaging systems used in this thesis are very well described in [12].

**Absorption Imaging** Absorption imaging views the shadow cast by the atoms, and through computer manipulation, is displayed as a bright spot in order to be more visually appealing. It has the ability to give a spatial view of the dipole trap, and has a very high sensitivity making a good detection scheme for small traps. MOT repump light is used, which implores the atoms be pumped into their lower state before imaging. This technique was used predominantly in the alignment of the trap, because of its ability to provide spatial definition of the various trapping beams.

**Flourescence Imaging** Unlike absorption imagine, the basis of flourescence imaging is the collection of photons scattered from the atoms in the trap. This is done by comparing an image of the MOT loaded under normal conditions, to an image on the MOT loaded with the atoms from the dipole trap already in place. The difference in the images (once calibratead, see below) provides a quantitave value of the number of atoms in the trap. Flourescence imagine was used primarily in the optimization of trap, in order to gauge the effect of parameter changes on the total number of transferred atoms.

### 4.2.1 Rb85 Atom Number to Fluorescence Calibration

The number of atoms trapped in a MOT or optical dipole trap can be calculated based on the fluorescence of the atoms as detected on a CCD camera or photo detector if one knows the fraction of light reaching the detector ( $\eta$ ), the loss of the optical system ( $L$ ), the response of the detector ( $R$ ) and the energy scattered by a single atom (related to the scattering rate,  $\Gamma_{\text{scatt}}$ ). The total number of atoms is given by:

$$N_{\text{atoms}} = \frac{V_{\text{pd}}}{L \cdot R \cdot \eta \cdot \left(\frac{hc}{\lambda} \cdot \Gamma_{\text{scatt}}\right)} \quad (4.1)$$

The number of atoms can also be related to the measureable summed pixel count found via recapture imagine through the correlation between measured voltage and summed pixel count.

**Fractional Area** Only a small portion of the emitted light reaches the first lens of the optical system, which is situated 129mm from the MOT center. One inch optics were employed in the optical system which gives a diameter of 23mm after accounting for loss around the edges of the components. Thus, the fractional area seen by the photodetector is:

$$\eta = \frac{A_{\text{pd}}}{A_{\text{tot}}} = \frac{\pi r_{\text{pd}}^2}{4\pi r_{\text{tot}}^2} = 1.98 \times 10^{-3} \quad (4.2)$$

**Loss due to Optical System** To avoid approximations of the loss due to the many optical components in the system, the photodetector was calibrated with as many optical components as possible in place (beam splitter, band pass filter, and two lenses). Although the bandpass filter does reduce the fluorescence that reaches the photodiode, it plays an important role in ensuring that the Rb photo detector only detects Rb fluorescence, and the Li photodetector (placed on the

## 4.2. Imaging

other output - the transmission axis - of the cube beam splitter) only detects Li fluorescence. In a single species MOT, this is not crucial. However, in a dual species MOT, the ability to separate the fluorescence from each species is important in determining the individual MOT sizes. This leaves only the reflection from the MOT cell to be accounted for. The photodetector sits at an angle of  $14^\circ$  to the vertical axis, creating a 12% loss due to reflection. Thus:

$$L = .88 \tag{4.3}$$

**Response of Photodetector** Collimated Rb pump light (tuned to the  $5S_{1/2} \rightarrow 5P_{3/2}$  resonance) was used to simulate the MOT fluorescence, and calibrate the photodetector response to the incident light with most of the optical components in place. Due to a small beam waist and collimation, it can be said with confidence that there was no loss due to scattering off the sides of the optical telescope. Note that the beam splitter does not split the light at exactly 50% in each direction. This calibration was done with the Rb photodetector receiving the reflected light from the cube beam splitter. Figure 4.1 shows the plot and fit of the photodetector response (note error was given for incident light, not output voltage) so that the linear fit was inverted to give the response of the photo detector:

$$R = 0.0169 \quad \left[ \frac{\text{V}}{\text{nW}} \right] \tag{4.4}$$

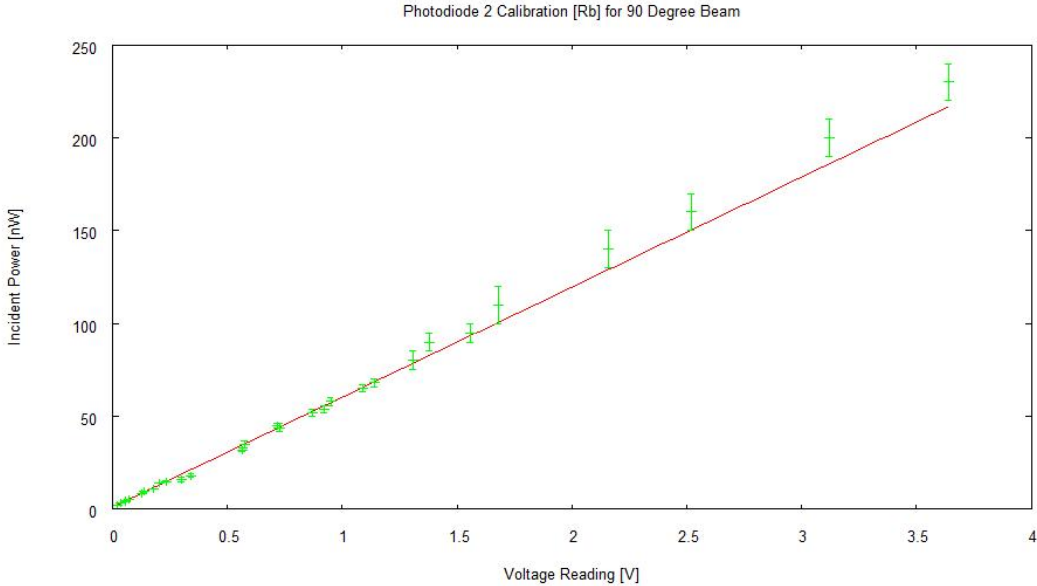


Figure 4.1: Calibration of photodiode with optics in place.

**Scattering Rate** The scattering rate is given by (with all frequencies given in units of angular frequency):

$$\Gamma_{\text{scatt}} = \frac{\gamma}{2} \cdot \frac{s}{1 + s + \left(\frac{2\delta}{\gamma}\right)^2} \tag{4.5}$$

where  $\gamma = 2\pi \cdot 6.06 \times 10^6$  Hz is the natural line width of the transition,  $\delta = 2\pi \cdot 11 \times 10^6$  Hz is the detuning of Rb pump light, and  $s = I/I_{\text{sat}}$  with  $I_{\text{sat}} = 3.58$  mW/cm<sup>2</sup> [15].

## 4.2. Imagining

---

**Intensity of MOT Light** To find the intensity of light illuminating the atoms in the MOT (as opposed to total power) a 7mm diameter aperture was placed over the power meter (to give a common area of measurement), and the laser beams entering the MOT region were measured. The intensity of each beam was assumed constant over that area. To account for loss of light due to the MOT cell, the total power was measured before and after the cell (a total of four interface passages for the x and y axis) and the loss per interface was calculated based on these values. As the z-axis hits the cell perpendicular to the direction of travel, the loss at the cell is assumed to be 10% over two interfaces. Values of the interface loss on the x and y axis are shown in Table 4.1 and the values of the intensity of each of the 6 beams at the MOT are given in Table 4.2. Note, for the x and y axis, the first beam passes through two interfaces, while the reflected beam passes through six interfaces. One finds, for the current setup:

$$s = 13.83 \tag{4.6}$$

Axis	Before Cell [mW]	After Cell [mW]	Total Loss	Transmission Per Interface
X	1.4	1.1	.214	.941
Y	13.4	9.7	.276	.922

Table 4.1: Power loss at MOT Cell. For Reference, the transmission per interface on the z axis (that is, perpendicular to the cell) is .949

Axis	Beam 1 [mW/cm <sup>2</sup> ]	Beam 2 [mW/cm <sup>2</sup> ]	Total Intensity
X	1.84	1.44	3.28
Y	18.11	13.09	32.91
Z	8.17	5.13	13.31
Total	-	-	49.50

Table 4.2: Intensity of each MOT beam at the MOT center.

Finally, using the above values, the scattering rate is:

$$\Gamma_{\text{scatt}} = \frac{\gamma}{2} \cdot \frac{s}{1 + s + \left(\frac{2\delta}{\gamma}\right)^2} = 9.399 \times 10^6 s^{-1} \tag{4.7}$$

**Number of Atoms based on Voltage** Based on the output voltage of the photodetector, and the values calculated above, the number of trapped atoms is given by:

$$N_{\text{atoms}} = 1.41 \times 10^7 \cdot V \tag{4.8}$$

Where V is given in Volts. For reference, a typical 50mV trap contains  $9.6 \times 10^5$  atoms.

**Number of Atoms based on Pixel Count** An easily measured indicator of trap size is the summed pixel count of a recapture fluorescence image. To convert from voltage to pixel count, a relation between the voltage and pixel count was found by varying the MOT loading times. The exposure time of the camera was 10ms, in addition to the 10ms it takes for the aperture to fully open. The recapture imaging code used in this calibration was structured such that the recapture of atoms began as soon as the camera shutter was fully open, as opposed to occurring while

## 4.2. Imaging

the shutter was opening. Clearly, the following relationship is only valid under these described conditions. This relation is seen in Figure 4.2 and gives the scaling relationship (again, inverted from the figure fit):

$$R_{\text{pixel}} = 1.06 \times 10^{-7} \frac{V}{N_{\text{pixel}}} \quad (4.9)$$

Where  $N_{\text{pixel}}$  is the summed pixel count. Thus, the number of atoms is related to the summed pixel count (oddly and neatly enough) by:

$$N_{\text{atoms}} = 1.50 \cdot N_{\text{pixel}} \quad (4.10)$$

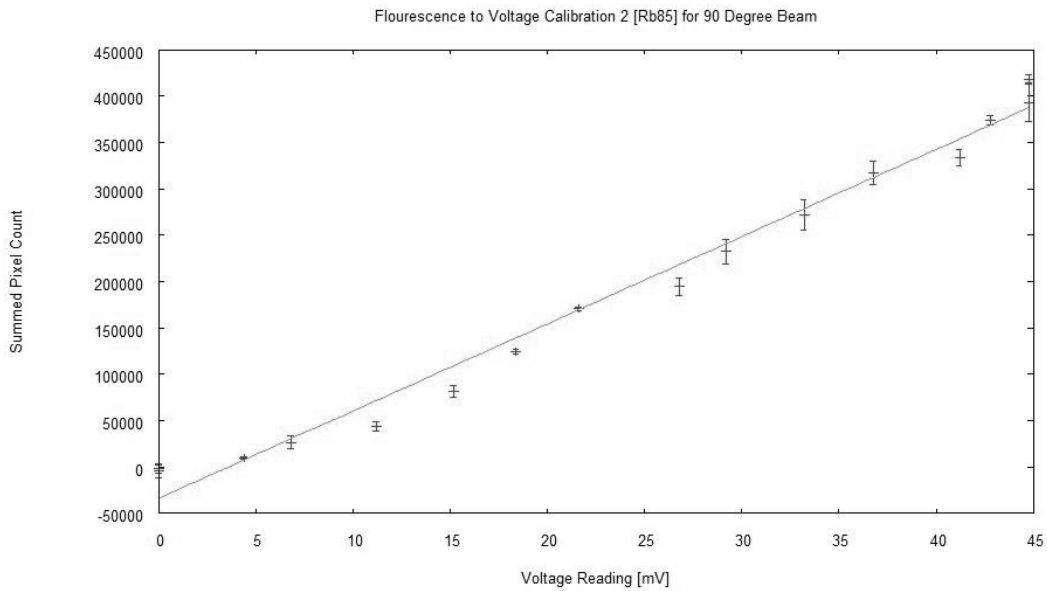


Figure 4.2: Calibration of summed pixel value to voltage reading on oscilloscope. Error on summed count given by standard deviation of three separate fluorescence images of the MOT

A full description of the calculations described above can be found in Appendix B.

# Chapter 5

## Results

A full schematic of the experimental setup can be found in Appendix A.

Trapping was originally achieved in only a single beam configuration, using the beam path currently employed by the first arm of the cross trap. However, since the process of alignment and data collection is equivalent for this (now defunct) setup, and the final cross trap, the cross trap will be the focus of the discussion of alignment, along with the trapping parameters and optimization. Data was taken for each arm individually, in order to understand and quantify possible differences between them, in addition to the cross trap.

### 5.1 Trap Alignment

Initial alignment of the trapping beam to the MOT was done via imaging the MOT fluorescence and trapping beam on the far side of the MOT cell. Due to space considerations, a  $45^\circ$  mirror was used to reflect the light upwards into an adjustable camera mounted on the frame structure. The mirror is not fixed, and can be moved as needed in order to image the first and second arm. In this setup, the trapping beam can be ensured to pass through the atoms in the MOT when the two images overlap on the alignment camera. The overlap can be achieved by either adjusting the mirror or beam splitter (for arm one and two respectively) that direct the beam towards the cell, or by moving the trap loading position of the MOT via changes in the compensation coil current amplitudes.

To a first approximation, the crossing of all three beams (two from the SPI laser, and a third from the IPG laser) was realized first overlapping the MOT and the IPG beam on its alignment camera. Then, the SPI beams were moved to overlap the MOT at this setting. At minimum, due to the large size of the beam on the camera, this process guarantees that the three beams come close to overlapping in space, but says nothing about the relative location of their foci.

As the Raleigh Range of the trapping beams is on the order of a few millimetres, the trap is very sensitive to the longitudinal position of the focus within the cell. In order to be able to explore the full range on movement of the focus, multiple possible loading positions (defined as a compensation coil setting where the beam and MOT image overlap) were taken over the entire range of movement of each lenses translation stage.

Once trapping was seen in both individual beams, a first attempt was made at achieving a three beam cross trap [Fig. 5.1]. As seen, the three beams are not crossed at the same location, but were triangulated in space. The three spots in Fig. 5.1 are, from left to right: IPG beam crossing the second SPI arm, IPG beam crossing the first SPI arm, and the two SPI beams crossing with each other. From here, it is a simple task to shift the two SPI beams towards each other in order to create a single crossing of all three beams [Fig. 5.2].

## 5.1. Trap Alignment

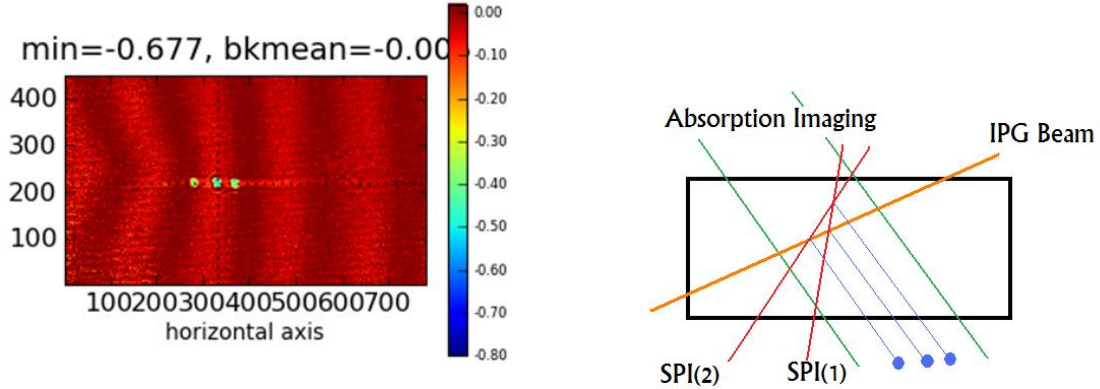


Figure 5.1: (Left) Image of first attempt at a three beam cross trap. The three spots are, in order of left to right, created by the crossing of: IPG + SPI(2), IPG + SPI(1), SPI(1) + SPI(2). (Right) Cartoon of beam geometry.

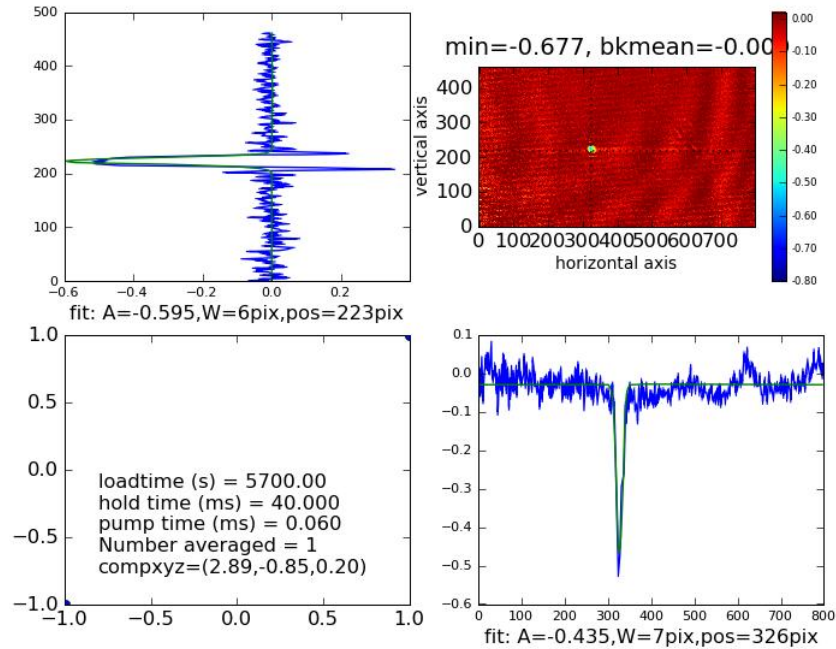


Figure 5.2: Three beam cross trap

In order to confirm the location of high absorption was, in fact, a crossing of all three beams, the three possible combinations of beams were imaged, each showing a crossing at the same location as Figure 5.2, confirming the existence of a three beam cross trap [Figures 5.3, 5.4 and 5.5].

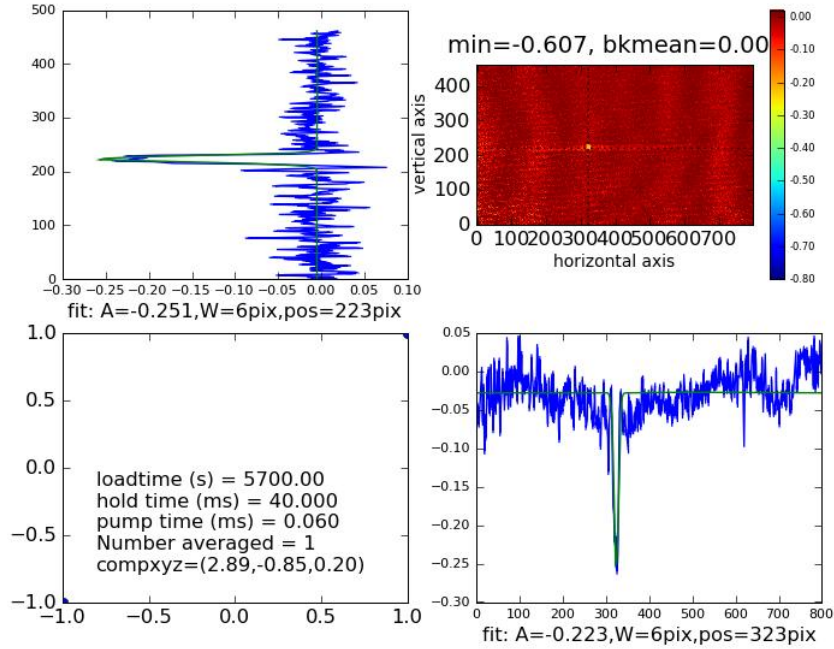


Figure 5.3: Crossing of IPG beam with the first beam arm from the SPI laser

## 5.2 Trap Parameters

### 5.2.1 Radial Trap Frequencies

Using the method of parametric excitation (discussed earlier) the trap frequencies of the single arm and cross traps were examined. Modulation of the laser power was achieved through a python script that generated set points on a sine wave (given an input frequency, amplitude, and modulation amplitude) and sent these values via an AO to the laser control. This acted to modulate the output power in a roughly sinusoidal manner. For all readings, the power was modulated by 15% in order to achieve a clear and notable trap loss, but (attempt) to keep the broadening of the line to a minimum. The trapping frequencies were investigated at 8.5W for the single arm trap [Fig. 5.6], and at 8.5W and 34W for the cross beam trap [Fig. 5.7]. These values were chosen in order to compare the frequencies of a single arm and cross trap at the same power, as well as giving the ability to see the effect of a four times increase in trapping power which should (and did) double the trapping frequency, according to (2.39).

The trapping frequencies for the single arm trap are 2kHz and 1.6kHz for the first and second arm respectively, as compared to the expected value of 1.9kHz. The first arm compares well to the expected value. The lower value for the second arm suggests that the lens focuses the beam to a larger spot size. Based off of (2.39), the calculated values for the waist size from each arm are  $37.3\mu\text{m}$  and  $46.7\mu\text{m}$  for the first and second arm, respectively. However, the agreement with the first arm does reassure that there is minimal effect of the thermal lensing of the cell on the trapping beam. In addition, the larger size of the second arm waist confirms a difference in the

## 5.2. Trap Parameters

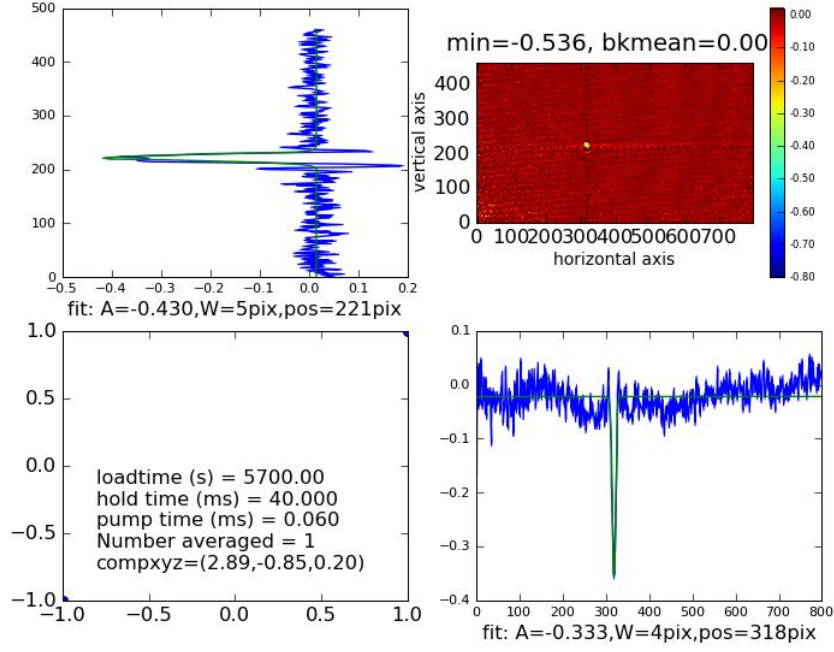


Figure 5.4: Crossing of IPG beam with the second beam arm from the SPI laser

spot size suggested by the differing focal lengths.

The trapping frequencies for the cross trap are 1.5kHz and 3.2kHz for 15W and 30W respectively, which are lower than the expected values of 1.9kHz and 3.9kHz. This can be attributed to, in part, the fact that there is no well defined radial direction in the cross beam trap, and the expect values were calculated based on the assumption of the same waist size as in the single arm trap. The lower trapping frequencies also suggests that the effects of the larger beam waist of the second arm carry over to the cross trap.

Because not all atoms will sit in the very bottom of the trap, some will experience different trapping frequencies, especially if they sit outside of the location where the harmonic potential was assumed, which can account for a portion of the broadness. In addition, varying the power of the trapping beam will have the effect of spreading out the trapping frequency. From (2.39) the broadening of the of the 8.5W trapping frequency (with 15% modulation) line should be on the order of:

$$\Delta\omega_r = \left(1 - \sqrt{\frac{9.775}{7.225}}\right) \cdot \omega_r = (0.16)\omega_r = 0.3\text{kHz} \quad (5.1)$$

and the 34W line on the order of:

$$\Delta\omega_r = \left(1 - \sqrt{\frac{39.1}{28.9}}\right) \cdot \omega_r = (0.16)\omega_r = 0.6\text{kHz} \quad (5.2)$$

The broader line can be seen clearly in Figure 5.7. In addition, this broadening explains the blurring of the high frequency cut-off. That is, in the parametric heating method modulation at

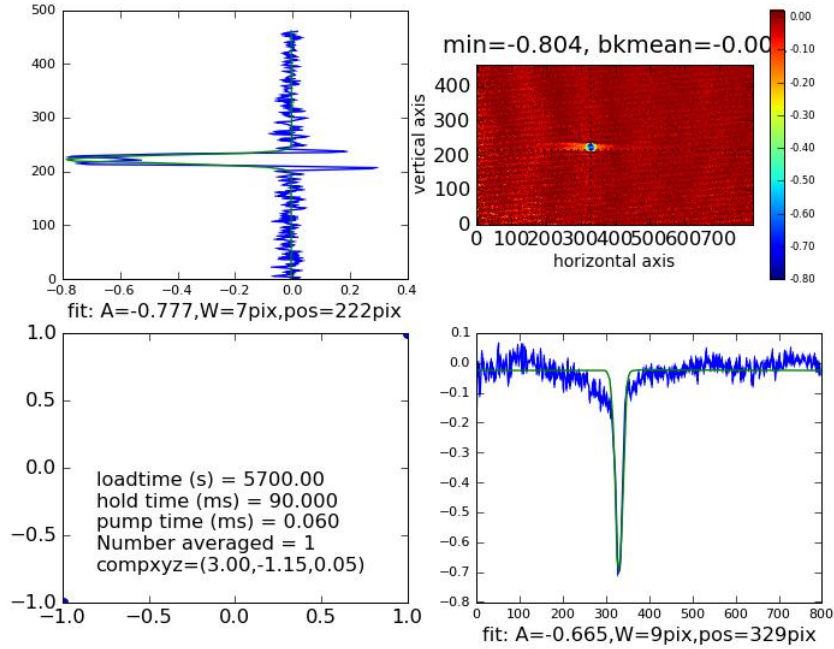


Figure 5.5: Crossing of the two SPI beams

frequencies greater than twice the trapping frequency should not heat atoms. Thus, one would expect a non-symmetric dip in remaining atom number with a sharp increase when moving towards higher frequency. However, this cut-off is (slightly) blurred out due to the broadening described above.

### 5.2.2 Hold Times

Measurements of the trap lifetimes were taken for both the single (at 15W) and cross beam (15W and 30W) with a 100ms load time. The atoms were shelved into the lower hyperfine state by turning off the re-pump light 6ms before the pump light. This acts to kick atoms out of the upper hyperfine state  $|F = 3, M_F = 3\rangle$  into the lower hyperfine state  $|F = 3, M_F = 2\rangle$ . The result should be to increase the trapping lifetimes due to a decrease in inelastic collision which heat atoms, leading to trap loss.

Plots of atom number versus hold time are shown for both the single beam traps [Fig. 5.8] and cross beam trap [Fig. 5.9]. Both exhibit an interesting curve with non-exponential decay at short hold times, trending to an exponential decay at long hold times. This indicates that during the first one second of the traps life, the high densities initiate inelastic density dependant collisions that quickly reduce atom number. In addition, this may also indicate evaporation or photoassociation of the trapped atoms by the trapping laser. As the number of atoms within the trap decreases due to these loses (which is equivalent to a decrease in density, as the trap size is constant) the impact of the density dependant collisions is reduced, leading to a normal lifetime curve that exhibits a (generally) exponential decay.

## 5.2. Trap Parameters

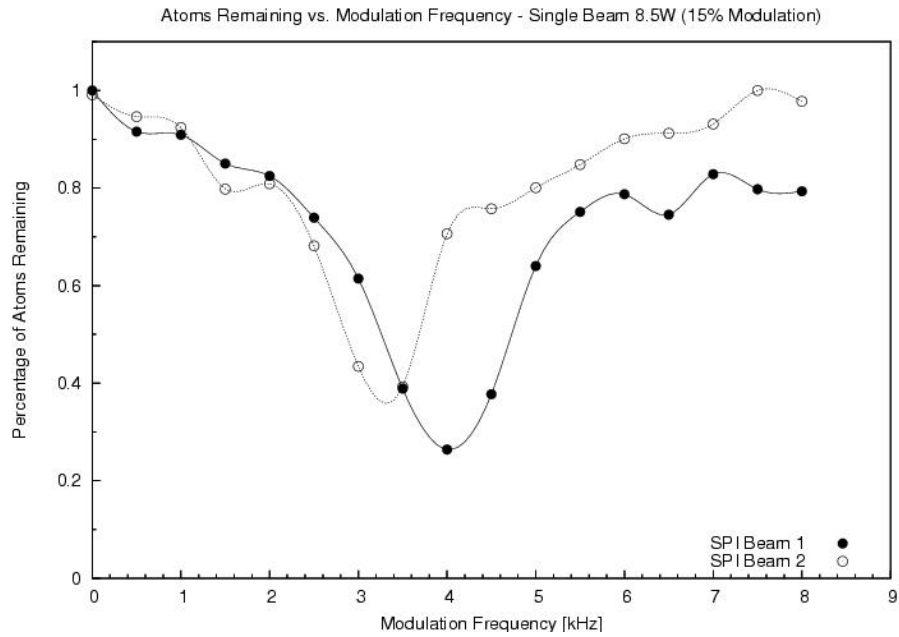


Figure 5.6: Radial trapping frequencies for the two single arm traps at 8.5W. Notice that the second arm has a lower radial frequency (1.6kHz) than the first (2kHz).

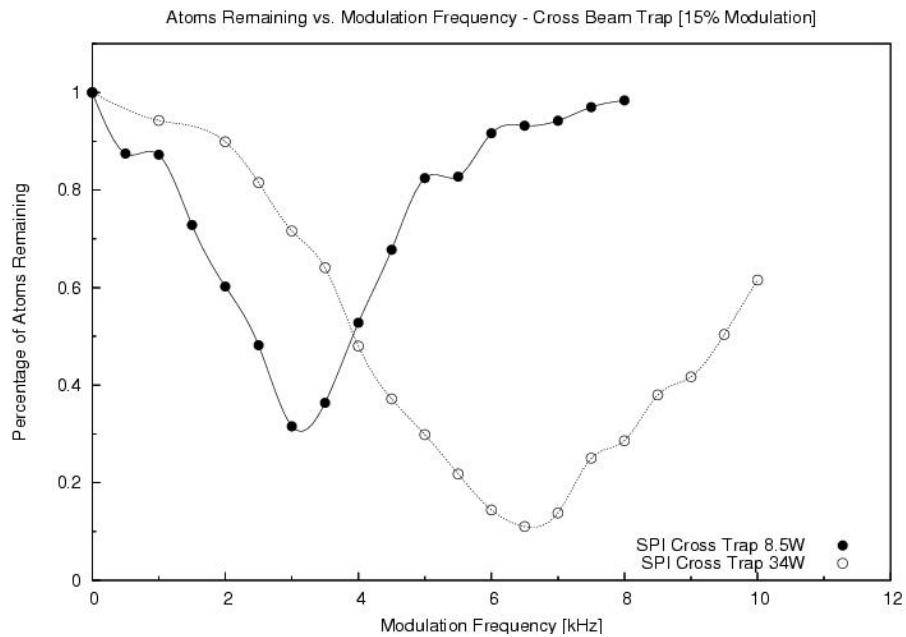


Figure 5.7: Radial trapping frequencies for the cross beam trap at 8.5W and 34W. Note the frequency doubles with a four times increase in trapping power, as expected, and is also a more broad feature.

Of note for the single beam traps is that the second SPI beam has a higher number of trapped

## 5.2. Trap Parameters

atoms at short hold times, but tends to the number in the first arm at long hold times. Again, this indicates a faster atom loss rate during the first seconds of the traps lifetimes due to a higher density in the trap. On the other hand, the cross beam traps (one at 15W, the other at 30W) contain roughly the same number of atoms in the early stages of their life, but the 15W trap loses atoms at a faster rate than its 30W counterpart. This can be explained by an increased trap depth in the 30W trap, which requires that atom undergo more collisions before obtaining a high enough energy to escape the trapping potential. This manifests itself as a longer trap lifetime, as seen.

For comparison, the IPG trap currently has lifetimes on the order of 15s. The relatively short lifetimes from the SPI traps are cause for further investigation. However, possible explanations include overall power fluctuations or possible polarization fluctuations (as discussed above).

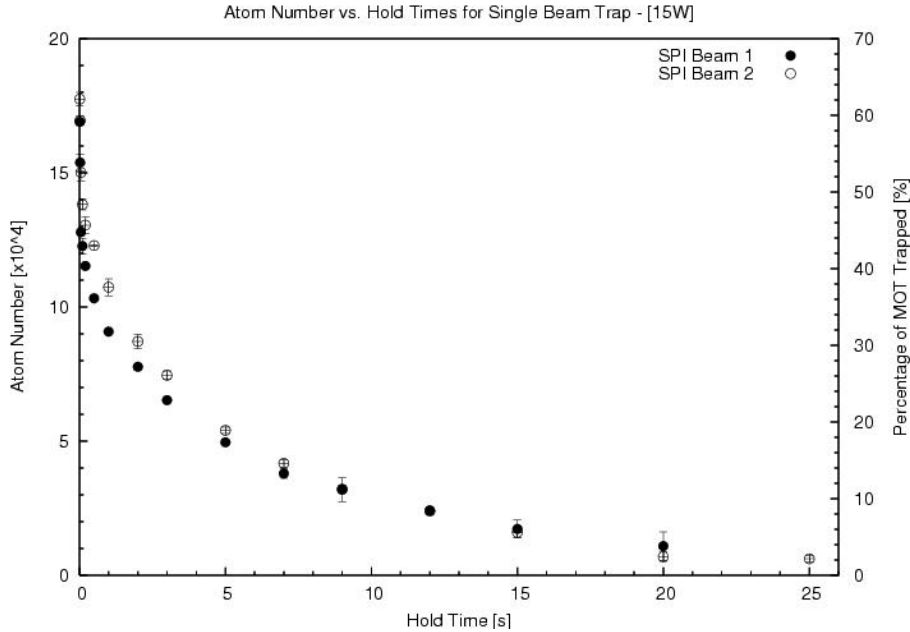


Figure 5.8: Trap lifetime curve, showing atom number vs. hold time for the two single beam arm traps at 15W,  $t_{\text{load}} = 100$  ms.

### 5.2.3 Atom Number vs. MOT Size

Trapping efficiency (that is, the atom of numbers transferred to the dipole trap relative to the total size of the MOT) appears to have a great deal of dependance on the size of the MOT at low MOT atom numbers ( $< 100000$  atoms) and tends to a transfer efficiency of 40% at larger sizes. There appears to be a linear correlation between the MOT size and number of atoms transferred to the dipole trap so one can easily predict future trap sizes for larger MOT atom numbers. Figure 5.10 shows the trend for the single arm traps at 15W, and Figure 5.11 shows the same data for the cross beam trap at 15W and 30W. These data runs were taken using a load time of 100ms, and a hold time of 200ms. The different MOT numbers were obtained by transferring atoms at different values for the MOT load time.

## 5.2. Trap Parameters

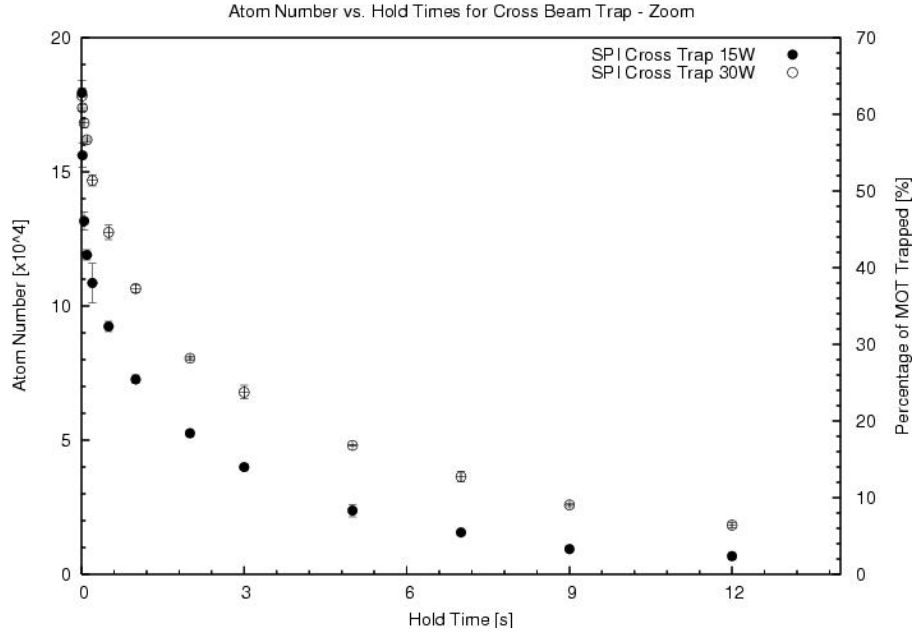


Figure 5.9: Trap lifetime curve, showing atom number vs. hold time for the cross beam trap at 15W and 30W,  $t_{\text{load}} = 100$  ms.

Of interest is to note that (at the same power) the single arm trap is consistently more efficient at loading atoms than the cross trap. Also of interest is the higher efficiency of loading (and total trap number difference for all MOT sizes) between the two single arm traps. Clearly, this again indicates a difference between the two arms most likely with regard to focus size.

### 5.2.4 Atom Number vs. Load Time

An examination of the number of trapped atoms as a function of the loading time can give important insight to the interesting physics occurring within the trap during the loading stage. Data taken for the single arm trap at 15W [Fig. 5.12] and cross trap at 15W and 30W [5.13] are shown. The hold time for the data sets is 200ms. All three curves show, generally, the same trend that can be nearly split into three relatively distinct sections:

**Initial Loading** For the first 50ms of the trap loading, atoms quickly fall into the trap at a large rate. At this early loading stage, density dependant loss rates from the trap are minimal, and the number of atoms increases nearly linearly with time. A linear fit to the early stage loading provides an estimate of the trap loading rates. The loading rate [Table 5.1] is fit for the data points contained within the first 50ms of trap loading. Of interest (again) is the difference in loading between the first and second single arm traps. It would also appear that the second arm dominates the loading characteristic of the cross trap which may, in part, be due to loading compensation coil settings or a difference in beam parameters. As well, it is clear from the loading rates of the two cross traps that a higher power (thus deeper) trap initially loads at a faster rate than the lower power cross trap, due to a greater trapping force.

## 5.2. Trap Parameters

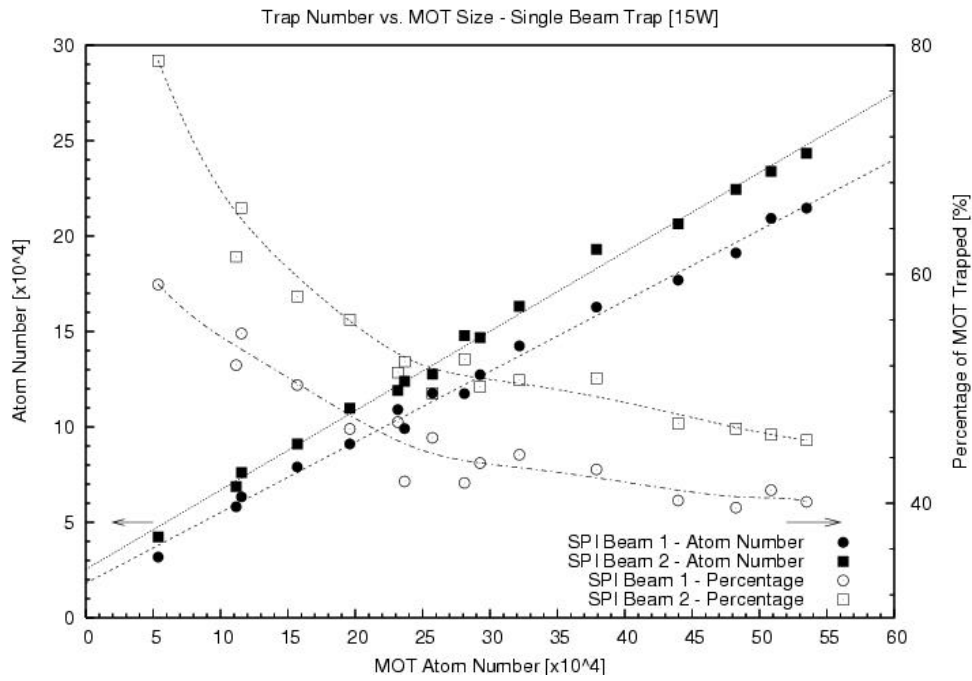


Figure 5.10: Trap number versus MOT Size for single arm trap

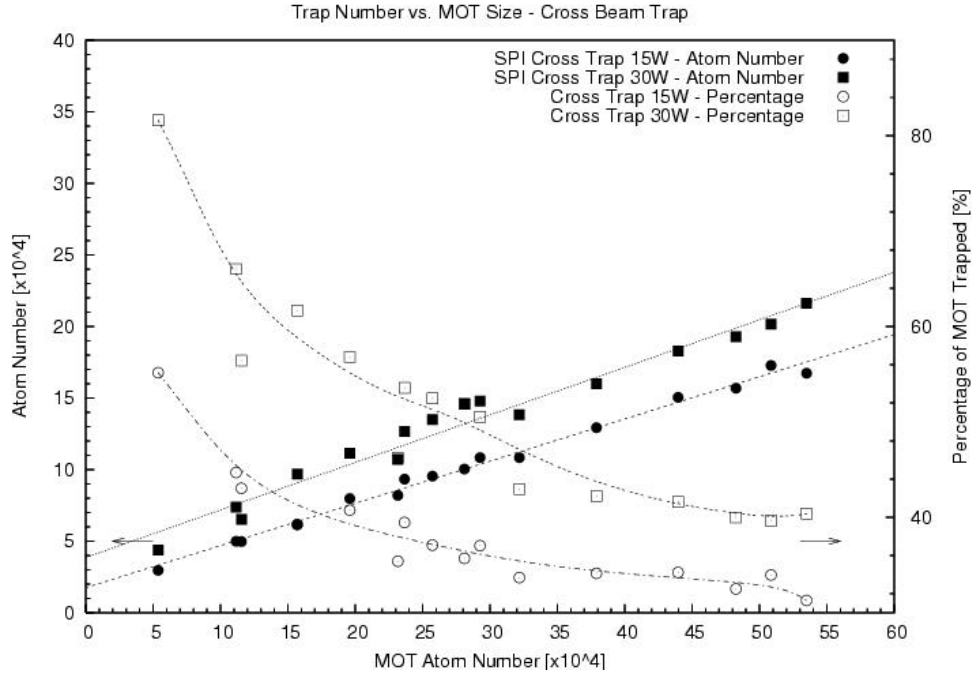


Figure 5.11: Trap number versus MOT Size for cross beam trap

## 5.2. Trap Parameters

Trap	Power	Load Rate [ $\times 10^3$ atoms/ms]
Single Arm - SPI One	15W	1.92
Single Arm - SPI Two	15W	2.57
Cross Trap	15W	2.52
Cross Trap	30W	3.11

Table 5.1: Initial loading rates for single and cross beam traps. Fit is to the first 50ms of loading, and turnover time indicates the time at which loss rates are larger than the transfer rate, causing a decrease in atom number for load time longer then this time.

**Temporary Equilibrium** Clearly, there reaches a point where the initial loading rate is exactly balanced by the loss rate from the dipole trap and the number of atoms holds roughly constant for a short period of time. The decreasing loading rate can be accounted for in two ways. First, the detuning of both the pump and repump light is closer to (or at resonance) with the resonance frequency in order to cool atoms. However, over time, this also leads a decrease in atoms in the MOT <sup>2</sup>. Secondly, as the dipole trap fills, the effect of density dependant collisions causes the overall MOT loss rate to increase. The effect is that the transfer rate into the MOT is balanced with the loss rate from the MOT and the trap, leading to a temporary equilibrium. Of interest is the spiked peak in the 30W cross trap, indicating that at high powers, the density dependant losses quickly overpower the loading rates, leading to a short (or near non-existent) steady state stage.

**Decay** Since the atom loss reduces the number of atoms in both the dipole trap and MOT, the reservoir of atoms in the MOT is depleted and the corresponding loading rate into the dipole trap drops continuously, the number of atoms transferred into the trap decreases with longer load times. This loss is dominated by collisional processes [8], and can be seen qualitatively via the faster decay seen in the denser 30W cross trap as compared to the 15W cross trap.

### 5.2.5 Atom Number vs. Power

The effect of increasing the trapping lasers power on the number of atoms trapped is shown for the single arm traps [Fig. 5.14] and cross beam trap [Fig. 5.15]. An important note is that the power displayed is the actual output power of the laser, which means for the single arm traps, the trapping power is half the listed value. The curves for both the single and cross beam traps show the same trend. No atoms are loaded until the trap depth is greater than the temperature of the atoms in MOT. Then, the trapped atom number increases exponentially for some range of powers, and finally grows linearly with increasing trap depth. Of greatest interest is explaining the leveling off at a certain power and, more importantly, the dip that occurs in the single beam traps when the power in the single arm is around 15W.

The dip in the power curve may have its roots in two different phenomena. First, the trap depth at certain powers may produce trap frequencies that are resonant with vibrations occurring within the room, leading to trap heating and loss. Losses of this type would occur during the hold time, where the MOT light is off. One would expect to see an increase in the depth of the dip of

---

<sup>2</sup>The contribution of this loss can be quantified independent of the loading rate by examining the effect of turning on the MOT light during the traps hold time on the number of atoms held in a trap [8].

## 5.2. Trap Parameters

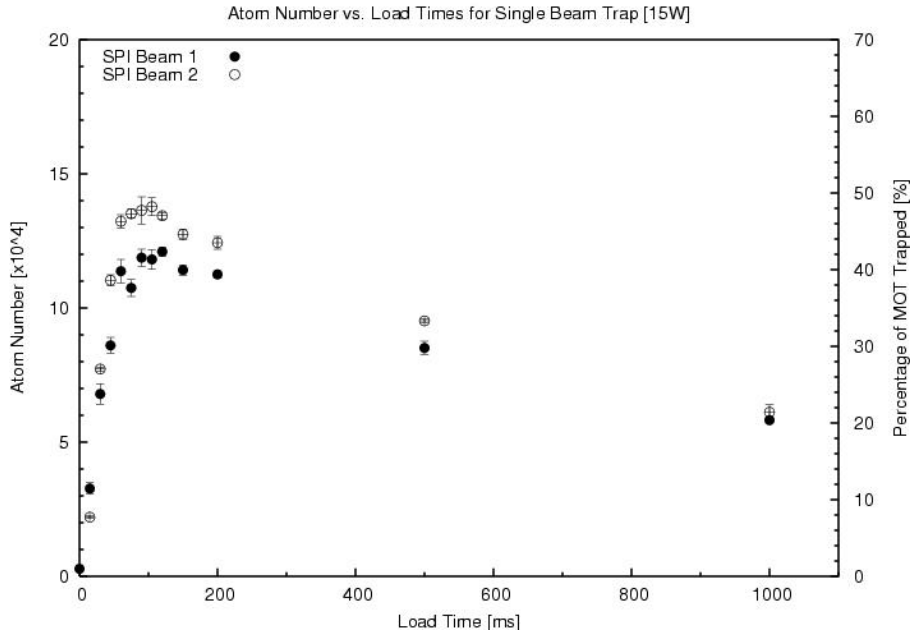


Figure 5.12: Loading curve for the two SPI single arm traps

these resonance powers with increasing hold time. Figure 5.16 shows that there is no change in the dip location or depth due to varying hold times, which rules out this explanation. In addition, the fact that the dip does not become more pronounced for longer hold times indicates that it arises from a loss mechanism that occurs before the holding time when the MOT light is still present

A second explanation involves the AC Stark Shift of the atomic energy levels due to the incident trapping light. During trap loading, the MOT pump light is set slightly red detuned (by 12 MHz) of the  $|F = 3\rangle$  to  $|F' = 4\rangle$  transition, while the repump light is set on resonance with the  $|F = 2\rangle$  to  $|F' = 3\rangle$  transition, with a much lower intensity. The incident trapping beam induces a differential AC Stark Shift in the atomic energy levels, with the effect of changing the energy of the states the MOT pump light couples. An example, shown schematically in Figure 5.17, is the MOT light now coupling the  $|F = 3\rangle$  to  $|F = 3\rangle$  transition, with a slight blue detuning. During the power interval where the light is blue detuned, heating of the atoms leads to a decrease in the number atoms in the MOT, manifesting itself as a loss in total atoms in the dipole trap. The same principle can be applied to the repump light. A simple test is to change the detuning of the pump and repump light. Moving to a bluer detuning would require a greater AC Stark Shift before the effect of heating appears, leading to the expectation of a shift of the dips position towards higher powers. The opposite applies for a redder detuning.

**Pump Light** No changes in the position of the dip were seen with changes of the MOT pump light detuning [Fig. 5.18]. This implies the pump light is not responsible for the dip. This statement is further validated by the lack of secondary dips at higher loading powers, where the pump light would move to being blue detuned of the  $|F = 3\rangle$  to  $|F = 2\rangle$  and  $|F = 1\rangle$  transition.

## 5.2. Trap Parameters

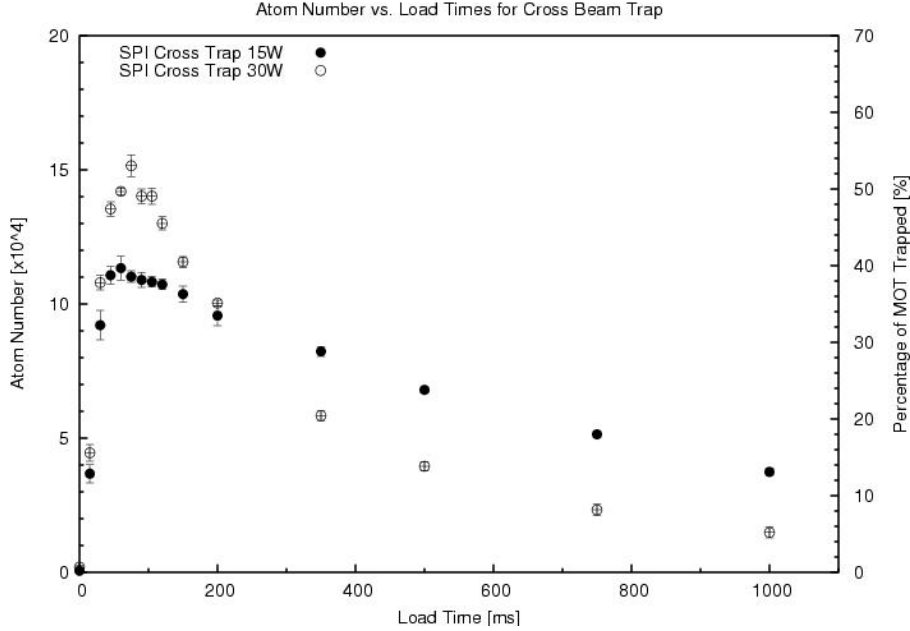


Figure 5.13: Loading curve for the cross beam trap at 15W and 30W. Note the faster decay in the 30W trap, indicating that collision processes dominate the loss rate during the loading stage.

**Repump Light** Large changes in the location (and size) of the dip were seen with changes to the detuning of the repump light [Fig. 5.19]. When a redder detuning was employed, the dip occurred at lower powers, as expected. A secondary dip, arising from the repump light coupling the population from the  $|F=2\rangle$  to the  $|F'=1\rangle$  state is not seen. However, as the splitting between these states is relatively small (29 MHz), the dip may be contained within the broad dip already seen. In addition, the dip occurs quite consistently at an effective detuning (taking into account the repump detuning and the differential AC Stark Shift) of 78MHz [Table 5.2]. Although this actually sits red detuned to the atoms at the center, it may be blue detuned for the majority of atoms sitting at slightly smaller differential detuning. In addition, 78MHz of effective detuning places the light slightly closer to the  $|F=2\rangle$  to  $|F'=1\rangle$  resonance, but well blue detuned, which could be another large contributor to the heating.

Repump Detuning	Dip Minimum [W]	Stark Shift [MHz]	Effective Detuning [MHz]
12	15	90	78
0	13	78	78
-6	12	72	78
-12	10.5	63	75

Table 5.2: Effective detuning of atoms in the trap during loading, induced by the differential AC Stark Shift and the detuning of the repump light, assuming a 60MHz Stark Shift at 10W of power.

The power difference between the two dips can also be used to find the relative difference in the waist of the two beam arms. Given the intensity of a Gaussian beam from (2.33) with

## 5.2. Trap Parameters

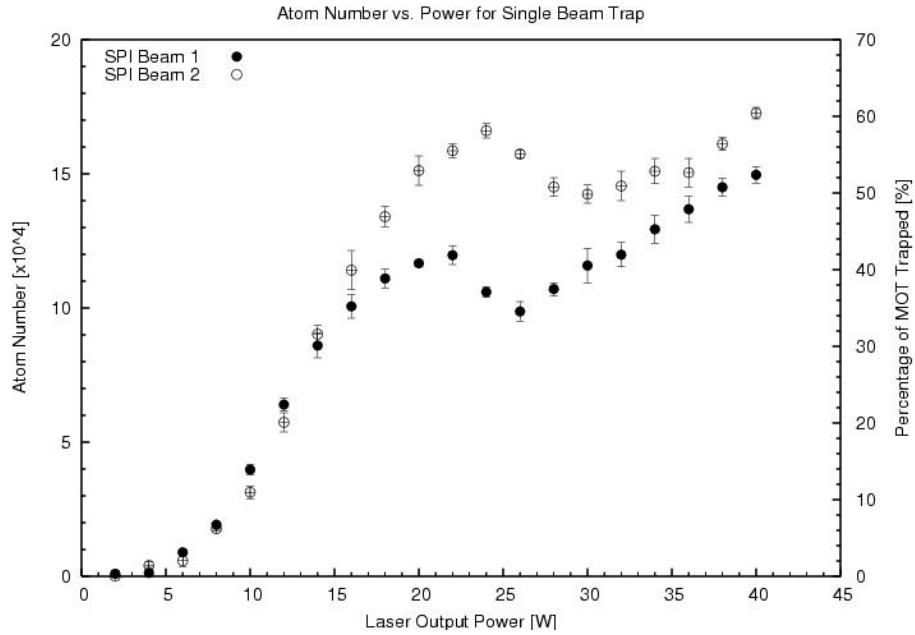


Figure 5.14: Effect of increasing power on the single arm traps. Notice an initial exponential increase, followed by trap number increasing linearly with trap depth.

$r = z = 0$  then the ratio of the beam waists is:

$$\frac{w_1}{w_2} = \frac{26\text{W}}{31\text{W}} = 0.839 \quad (5.3)$$

which is comparable with the value derived from the examination of the radial trapping frequencies of 0.799.

## 5.2. Trap Parameters

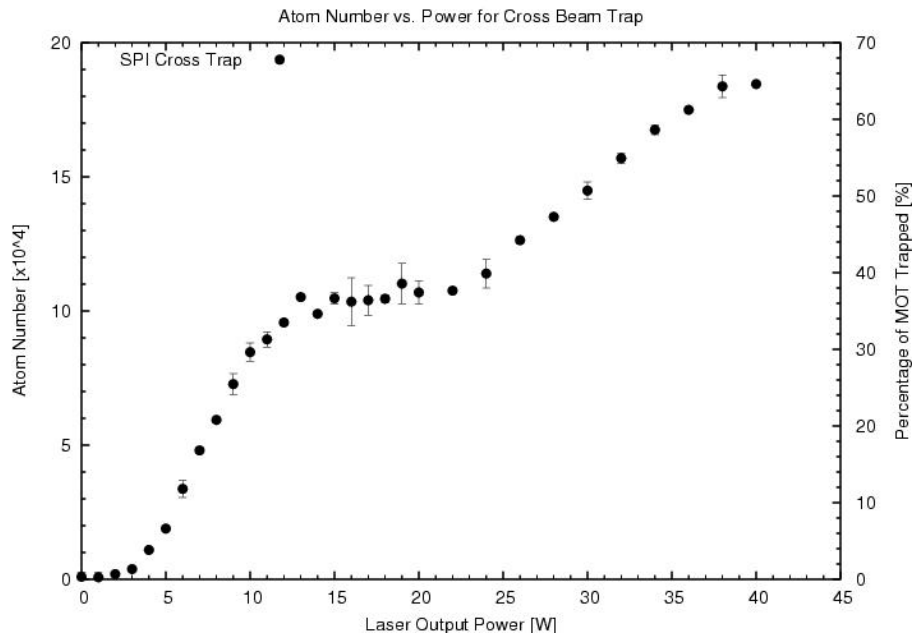


Figure 5.15: Effect of increasing power on the cross beam trap. Notice an initial exponential increase, followed by trap number increasing linearly with trap depth.

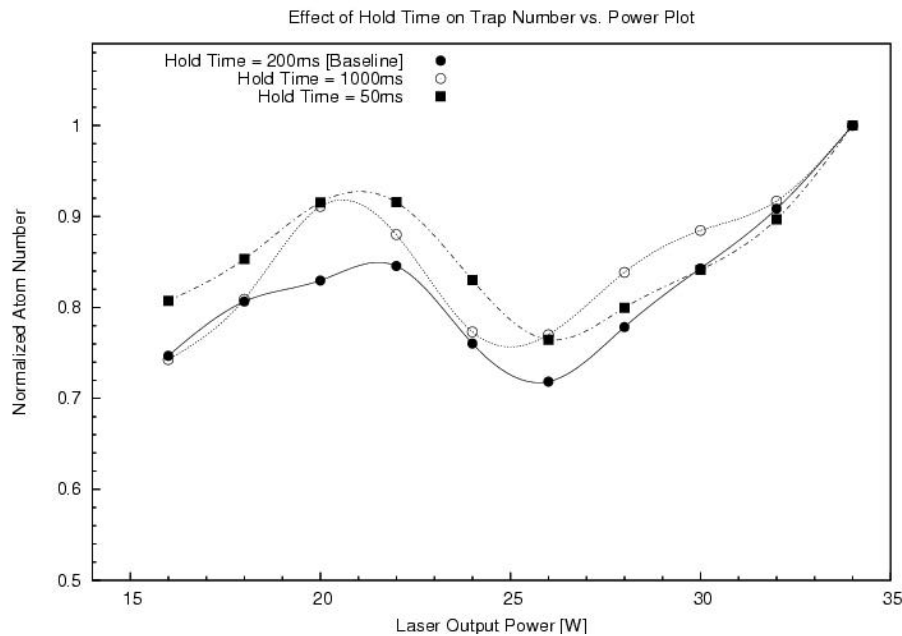


Figure 5.16: Effect of changing hold time on a subsection of the atom number versus power curve. Atoms number is expressed as a fraction of max atom number for visual ease, as changing hold times has the effect of lowering or raising the total number of atoms. The fact that the dip does not become more pronounced for longer hold times indicates that it arises from a loss mechanism that occurs before the holding time when the MOT light is still present

## 5.2. Trap Parameters

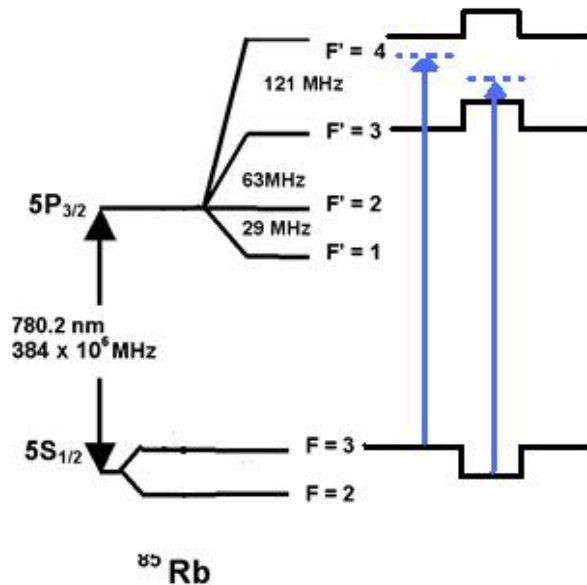


Figure 5.17: The AC Stark Shift induced by the incident trapping light acts to couple different resonant transitions with either blue or red detuning. For cases where the coupling is blue detuned, heating causes atom number to decrease. Shown here is the MOT pump light before (left arrow) and after (right arrow) the trapping beam is turned on.

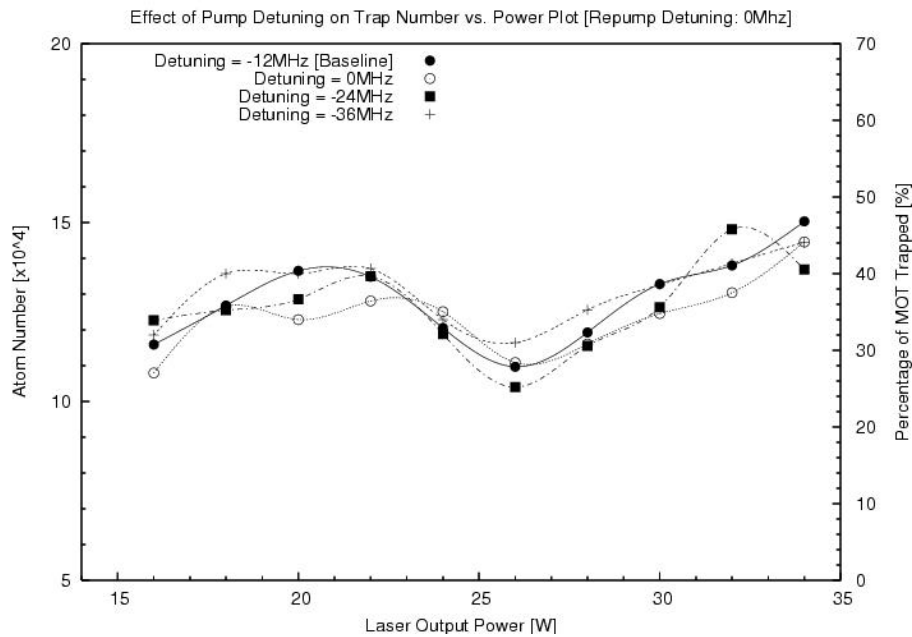


Figure 5.18: Effect of varying the MOT pump light detuning on a subsection of the atom number versus power curve, for SPI beam one. The lack of change in the dip implies that the MOT pump light is not responsible for the dip in atom number.

## 5.2. Trap Parameters

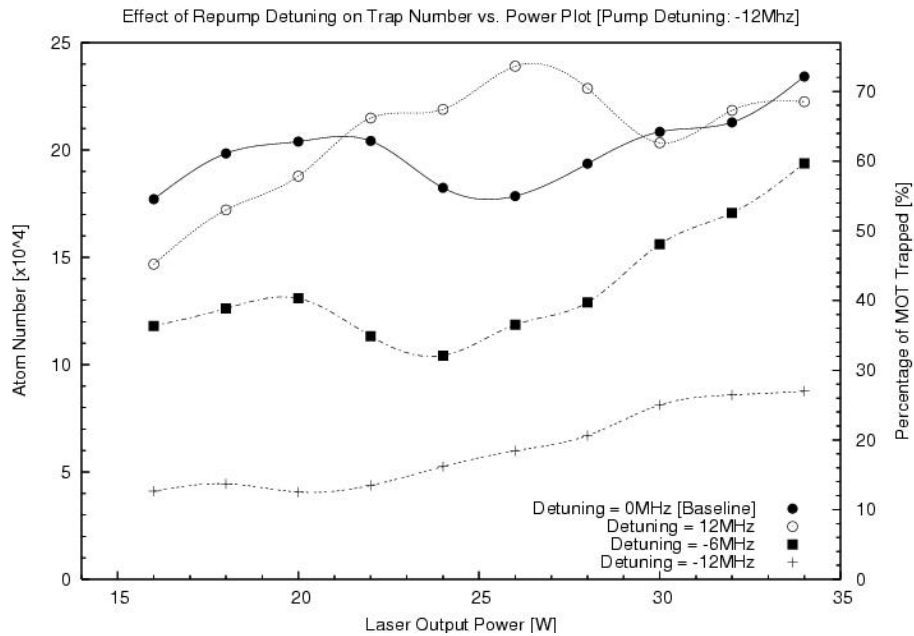


Figure 5.19: Effect of varying the MOT repump light detuning on the atom number loaded versus power for SPI beam one.

## Chapter 6

# Future Considerations

With an established and working cross beam trap, direct future work on the optical dipole trap consists of optimizing the transfer of atoms from the MOT to the trap. The clear dependence of the trapped atom number of the repump light shows great promise in the creation of a dark spot MOT, in order to reduce light induced losses during the loading of the trap. In addition, a more in depth understanding of the trapping physics can be obtained for a closer examination of the losses due to the repump light. In particular, whether the losses are caused by light interactions during loading, or an after effect of the light appearing during the storage time. Also of great importance is trying to further understand the short hold times of the trap, and find ways to improve them.

Motivated by [8], other trap parameters (outside of those discussed in this thesis) can be used to increase the transfer efficiency. These include: intensity and detuning of the MOT light, varying the magnetic field gradient and a greater effort in the location of the trap with respect to the MOT during loading. Finally, the effects of everything previously discussed with respect to different beam geometry (i.e., a smaller waist size) are to be investigated through the use of the beam expander that came with the laser.

As it has been noted, all the data contained within this thesis is for Rubidium. Lithium, which is much harder to trap because of its light weight and high MOT temperature is the next step in the experiment. With the cross beam trap, the achievable trap depths make it quite reasonable to expect to be able to trap Lithium. Furthermore, once both species are trapped, different methods to cool both Li and Rb to lower temperatures can be implemented, such as evaporative and sympathetic cooling.

# Chapter 7

## Conclusions

A flexible optical dipole trap, with the option of being used as a single or cross beam trap was created out of a 100W fibre laser. The final design consisted of two beam arms crossing at a shallow angle. Though the two beam arms are focused through two lens of similar focal length, experimental data suggest that the actual waist size varies by nearly 25%, with the first arm focusing to a spot size of  $37\mu\text{m}$  and the second to a spot size of  $46\mu\text{m}$ . These two beams are further overlapped with a separate trapping laser, giving the ability to trap and cool in the powerful SPI laser, and transfer atoms to the small bandwidth IPG laser for science.

Once trapping was achieved, the physical properties of the beam were examined through an investigation of hold times and trapping frequencies, and returned results consistent with expectations, under the assumption that the beams do focus to different sizes. This suggests the beams are not affected by the thermal lensing of the cell.

The transfer of atoms from the MOT to the optical trap was optimized by looking at a variety of parameters, including loading times, MOT pump and repump light detuning, power, and number of atoms in the MOT, as well as the location of the MOT with respect to the trapping beam. At the time of writing, the trap is capable of loading up to 80% of the Rb atoms contained in a MOT at low MOT sizes, and consistently 40% at large MOT sizes, with a lifetime on the order of 3-5 seconds. Trapping Li is left for work in the very near future.

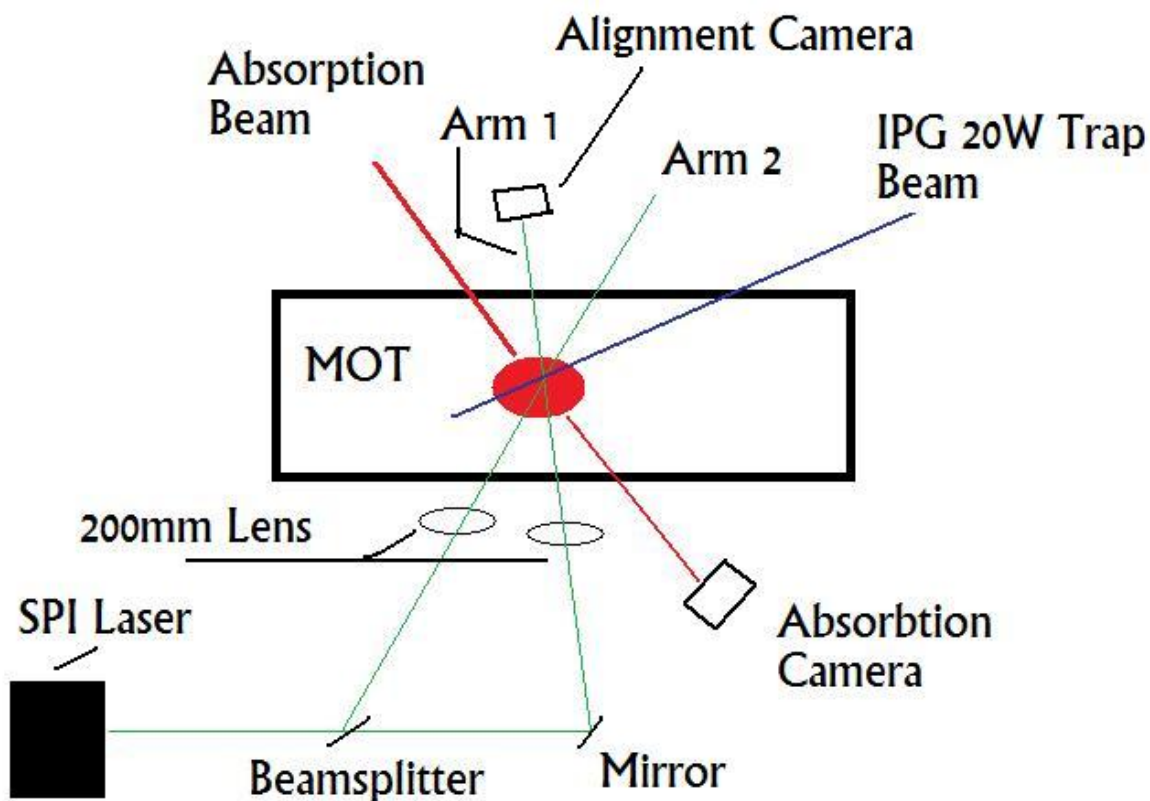
# Bibliography

- [1] H.J. Metcalf, P. van der Straten, *J. Opt. Soc. Am.* **20** 5, 887 (2003)
- [2] A. Fioretto, D. Comparat, A. Crubellier, O. Dulieu, F. Masnou-Seeuws, P. Pillet, *Phys. Rev. Lett.* **80** 20, 4408 (1998)
- [3] K.M. Jones, E. Tiesinga, P.D. Lett, P.S. Julienne, *Rev. Mod. Phys.* **87**, 483 (2006)
- [4] R. Grimm, M. Weidemöller, Y.B. Ovchinnikov, *Adv. At. Mol.* **42**, 95 (2000)
- [5] S. Kraft, M. Mudrich, K. Singer, R. Grimm, A. Mosk, M. Weidemöller, arXiv:physics/0109069v1 [physics.atom-ph] (2001)
- [6] D.A. Steck, *Quantum and Atom Optics* (2006)
- [7] K.M. O'Hara, Ph.D Thesis, Duke University, 2000
- [8] S.J.M. Kuppens, K.L. Corwin, K.W. Miller, T.E. Cjupp, C.E. Wieman, *Phys. Rev. A.* **62** (2000)
- [9] D.J. Griffiths, *Intro to Electrodynamics* (Pearson, NJ, 1999) p. 462
- [10] K.M. O'Hara, S.R. Granade, M.E. Gehm, T.A. Savard, S. Bali, C. Freed, J.E. Thomas, *Phys. Rev. Lett.* **82** 21, 4204 (1999)
- [11] D.J. Griffiths, *Intro to Quantum Mechanics* (Pearson, NJ, 2005)
- [12] M. Gao, Honors Thesis, UBC, 2008
- [13] R. Jauregui, arXiv:physics/0104075v1 [physics.atom-ph] (2001)
- [14] SPI Laser, SP-100C-0013-R00006 Manual
- [15] Daniel A. Steck, 'Rubidium 85 D Line Data' available online at <http://steck.us/alkalidata> (revision 0.2, 1 September 2008).
- [16] S. Chaudhuri, S. Roy, C.S. Unnikrishnam, *J. Phys: Conference Series* **80** (2007), 012036.

## Appendix A

# Experimental Setup Schematic

Schematic of the experiment setup, looking down on the optical table. Fluorescence imaging system is located above the MOT cell (not shown in this picture). A removable beam dump placed in the path of one of the beam arms can control which single beam trap is employed.



## Appendix B

# Rb85 Atom Number to Fluorescence Calibration Calculations

The following pages contain the Maple code displaying the details of the calculations relation the Rb85 atom number to the summed pixel count from the Apogee CCD camera.

## Constants

$$\delta := 2 \cdot \pi \cdot 5 \cdot 10^6 :$$

$$NL := 2 \cdot \pi \cdot 6.06 \cdot 10^6 :$$

$$Isat := 3.58 :$$

$$c := 3 \cdot 10^8 :$$

$$h := 6.626068 \cdot 10^{-34} :$$

$$\lambda := 780 \cdot 10^{-9} :$$

## Values

$$r_{pd} := \frac{23}{2} : \text{ #radius of the photodiode apperture}$$

$$r_{tot} := 129 : \text{ # distance from the MOT to the PD apparatus}$$

$$L := .88 \text{ # total fluorescence light transmitted through MOT cell}$$

0.88

$$\delta := 2 \cdot \pi \cdot 11 \cdot 10^6 : \text{ # MOT light detuning}$$

## Fractional Area

$$Af := \frac{\pi \cdot r_{pd}^2}{4 \cdot \pi \cdot r_{tot}^2}$$

$$\frac{529}{266256}$$

$$\text{evalf}\left(\frac{Af}{10^{-3}}\right) :$$

## PD Response

$$A := 59.2425 : \text{ # A,B are fits of the response of the PD.}$$

$$B := 1.05955 :$$

$$V := \frac{(P - B)}{A} :$$

$$R_1 := \frac{1}{A}$$

$$0.0168797738$$

$$R_o := \frac{B}{A}$$

$$0.0178849643$$

## Scattering Rate

### Intensity and Loss

$$Tx := .941 :$$

# MOT light transmission through MOT cell for each light axis

$$Ty := .922 :$$

$$Tz := .948 :$$

$$r_{app} := \frac{.7}{2} : \# \text{ radius of the apperture used to measure total power}$$

$$Px := .8 : \\ \# \text{ power of light in each axis BEFORE reaching MOT cell for} \\ \text{the first time}$$

$$Py := 8.2 :$$

$$Pz1 := 2.2 :$$

$$Pz2 := 3.5 :$$

$$Ix := \frac{Px \cdot (Tx^2 + Tx^6)}{\pi \cdot r_{app}^2} :$$

*# Total power in x axis. First beam passes through two surfaces, and the reflected beam passes through six surfaces*

$$\text{evalf}(Ix)$$

3.28395176

$$Iy := \frac{Py \cdot (Ty^2 + Ty^6)}{\pi \cdot r_{app}^2} :$$

$$\text{evalf}(Iy)$$

32.9062920

$$Iz := \frac{(Pz1 + Pz2) \cdot Tz^2}{\pi \cdot r_{app}^2} :$$

$$\text{evalf}(Iz)$$

13.3108432

$$s := \frac{(Ix + Iy + Iz)}{Isat} :$$

$$\text{evalf}(s)$$

13.8271192

### Scattering Calc

$$R_{scatt} := \left( \frac{NL}{2} \right) \cdot \left( \frac{s}{1 + s + \left( \frac{2 \cdot \delta}{NL} \right)^2} \right)$$

$$\frac{2.63241408810^8}{3.723044582 + \frac{43.43917637}{\pi}}$$

$$\text{evalf}(R_{scatt})$$

1.49993704310<sup>7</sup>

**Number of Atoms [Voltage] - 10<sup>9</sup> Factor due to convernsion from W to nW**

$$N_v := \frac{(Voltage)}{L \cdot R_1 \cdot Af \cdot \left( \frac{h \cdot c \cdot R_{scatt}}{\lambda} \cdot 10^9 \right)} :$$

*evalf(N<sub>v</sub>)*

8.86418609710<sup>6</sup> Voltage

### **Number of Atoms [Pixel Count]**

*VoltP := 9.13 · 10<sup>-8</sup> PixCount*  
*# Fit of relationship between the flourescence pixel count of the scope voltage.*

9.13000000010<sup>-8</sup> PixCount

$$N_p := \frac{(VoltP)}{L \cdot R_1 \cdot Af \cdot \left( \frac{h \cdot c \cdot R_{scatt}}{\lambda} \cdot 10^9 \right)} :$$

*evalf(N<sub>p</sub>)*

0.8093001909PixCount

## Appendix C

# Trap Depth and Frequency Calculation

The following pages contain a sample calculation displaying the Maple code used in finding the trap depths and frequency.

```

%%%%%%%%%%%%%%%%%%%%%%%%%%%%%%%%%%%%%%%%%%%%%%%%%%%%%%%%%%%%%%%%%%%%%%%%
%%                               Trap Depth Calc [Rb85]                               %%
%%%%%%%%%%%%%%%%%%%%%%%%%%%%%%%%%%%%%%%%%%%%%%%%%%%%%%%%%%%%%%%%%%%%%%%%

clear; Constant; warning off all;

%% booleans
%%%%%%%%%%%%%%%%%%%%%%%%%%%%%%%%%%%%%%%%%%%%%%%%%%%%%%%%%%%%%%%%%%%%%%%%
bool_ipg = 1;
bool_spi = 0;

P_output = [15];
AO_volt = [1.3];

%% spi calculations
%%%%%%%%%%%%%%%%%%%%%%%%%%%%%%%%%%%%%%%%%%%%%%%%%%%%%%%%%%%%%%%%%%%%%%%%
if bool_spi==1

waist_right = 37e-6;
waist_left = 46e-6;

trap_wl = 1090e-9;

w085 = (2*pi*c0)/(185);
w = (2*pi*c0)/(trap_wl);

rrange_right = (pi*waist_right^2)/(trap_wl);
rrange_left = (pi*waist_left^2)/(trap_wl);

k = 2*pi/trap_wl;

P = P_output*.915; % Power at atoms, accounting for loss at cell

I_left = (2*P(n)/2)/(pi*waist_left^2);
I_right = (2*P(n)/2)/(pi*waist_right^2);

V_left = ((3*pi*c0^2*Gamma85)/(2*w085^3))*((1/(w085-w))+(1/(w085+w)))*I_left;
V_right = ((3*pi*c0^2*Gamma85)/(2*w085^3))*((1/(w085-
w))+(1/(w085+w)))*I_right;

V_left_temp = (V_left/kB)*1000;
V_right_temp = (V_right/kB)*1000;

V_cross_temp = V_left_temp + V_right_temp;

freq_left_radial = (sqrt((4*V_left)/(m85*waist_left^2)))/(2*pi);
freq_left_axial = (sqrt((2*V_left)/(m85*rrange_left^2)))/(2*pi);
freq_right_radial = (sqrt((4*V_right)/(m85*waist_left^2)))/(2*pi);
freq_right_axial = (sqrt((2*V_right)/(m85*rrange_left^2)))/(2*pi);

end

```

```

%% ipg calculations
%%%%%%%%%%%%%%%%%%%%%%%%%%%%%%%%%%%%%%%%%%%%%%%%%%%%%%%%%%%%%%%%%%%%%%%%
if bool_ipg==1

waist = 39e-6;
trap_wl = 1064e-9;
w085 = (2*pi*c0)/(185);
w = (2*pi*c0)/(trap_wl);
rrange = (pi*waist^2)/(trap_wl);
k = 2*pi/trap_wl;

AO = .41*erf(1.73*AO_volt - 1.37)+.377 % Fit to the percent of total power
contained in the first order beam after passing through AO.
P = (P_output*AO*.65);

I = (2*P(n))/(pi*waist^2);
V = ((3*pi*c0^2*Gamma85)/(2*w085^3))*((1/(w085-w))+1/(w085+w))*I;
V_temp = (V/kB)*1000;

freq_radial = (sqrt((4*V)/(m85*waist^2)))/(2*pi);
freq_axial = (sqrt((2*V)/(m85*rrange^2)))/(2*pi);

V_temp_retro = 4*V;
freq_radial_retro = (sqrt((4*4*V)/(m85*waist^2)))/(2*pi);
freq_axial_retro = (k)*sqrt((2*4*V)/(m85))/(2*pi);

end

%% "Plot" to show the results
%%%%%%%%%%%%%%%%%%%%%%%%%%%%%%%%%%%%%%%%%%%%%%%%%%%%%%%%%%%%%%%%%%%%%%%%
if bool_ipg==1
figure(1); clf;
text(0,1, ['IPG Single Pass Trap Values'], 'FontWeight', 'bold');
text(0,.9, ['Laser Output = ', num2str(P_output), ' W']);
text(0,.85, ['Power at MOT = ', num2str(P), ' W']);
text(0,.75, ['Trap Depth = ', num2str(V_temp,3), ' mK']);
text(0,.65, ['Radial Freq = ', num2str(freq_radial*1e-3,3), ' x 2\pi
kHz']);
text(0,.60, ['Axial Freq = ', num2str(freq_axial,3), ' x 2\pi Hz']);

text(0,.5, ['IPG Retro Trap Values'], 'FontWeight', 'bold');
text(0,.4, ['Retro Radial Freq = ', num2str(freq_radial_retro*1e-3,3), '
x 2\pi kHz']);
text(0,.35, ['Retro Axial Freq = ', num2str(freq_axial_retro*1e-6,3), ' x
2\pi MHz']);
axis off
end

if bool_spi==1
figure(1); clf;

```

```

text(0,1, ['SPI Trap Values - Left Arm'], 'FontWeight', 'bold');
text(0,.9, ['Laser Output = ', num2str(P_output), ' W']);
text(0,.85, ['Power at MOT = ', num2str(P/2), ' W']);
text(0,.75, ['Trap Depth = ', num2str(V_left_temp,3), ' mK']);
text(0,.65, ['Radial Freq = ', num2str(freq_left_radial*1e-3,3), ' x 2\pi
kHz']);
text(0,.60, ['Axial Freq = ' num2str(freq_left_axial,3), ' x 2\pi Hz']);

text(.6,1, ['SPI Trap Values - Right Arm'], 'FontWeight', 'bold');
text(.6,.9, ['Laser Output = ', num2str(P_output), ' W']);
text(.6,.85, ['Power at MOT = ', num2str(P/2), ' W']);
text(.6,.75, ['Trap Depth = ', num2str(V_right_temp,3), ' mK']);
text(.6,.65, ['Radial Freq = ', num2str(freq_right_radial*1e-3,3), ' x
2\pi kHz']);
text(.6,.60, ['Axial Freq = ' num2str(freq_right_axial,3), ' x 2\pi
Hz']);

text(.3,.4, ['SPI Cross Trap Values'], 'FontWeight', 'bold');
text(.3,.3, ['Laser Output = ', num2str(P_output), ' W']);
text(.3,.25, ['Power at MOT = ', num2str(P), ' W']);
text(.3,.15, ['Trap Depth = ', num2str(V_cross_temp,3), ' mK']);

axis off
end

```